Geochemistry, Geophysics, Geosystems

RESEARCH ARTICLE
10.1029/2020GC009401

Key Points:

- We measure SKS splitting beneath the dense SEISConn array using several measurement methods.
- Splitting delay times decrease from west to east and fast directions are close to east-west.
- Our data shed light on both present-day mantle flow and past lithospheric deformation.

Supporting Information:

- Supporting Information S1
- Table S1
- Table S2
- Table S3

Correspondence to:
M. D. Long,
maureen.long@yale.edu

Citation:
Lopes, E., Long, M. D., Karabinos, P., & Aragon, J. C. (2020). SKS splitting and upper mantle anisotropy beneath the southern New England Appalachians: Constraints from the dense SEISConn array. *Geochemistry, Geophysics, Geosystems*, *21*, e2020GC009401. https://doi.org/10.1029/2020GC009401

Received 27 AUG 2020
Accepted 24 NOV 2020

SKS Splitting and Upper Mantle Anisotropy Beneath the Southern New England Appalachians: Constraints From the Dense SEISConn Array

Ethan Lopes[1,2], Maureen D. Long[2], Paul Karabinos[1], and John C. Aragon[2,3]

[1]Department of Geosciences, Williams College, Williamstown, MA, USA, [2]Department of Earth and Planetary Sciences, Yale University, New Haven, CT, USA, [3]Now at Earthquake Science Center, U.S. Geological Survey, Menlo Park, CA, USA

Abstract The geology of southern New England reflects subduction and terrane accretion during the Appalachian Orogeny and rifting during the breakup of Pangea. The presence of a low-velocity seismic anomaly in the upper mantle beneath New England suggests the possible presence of vertical mantle flow (upwelling). It remains poorly understood how the lithosphere beneath southern New England was deformed by past tectonic events; furthermore, the details of the present-day mantle flow field remain elusive. Observations of seismic anisotropy have the potential to constrain both past and present upper mantle deformation. Here, we present SK(K)S splitting observations at stations of the Seismic Experiment for Imaging Structure Beneath Connecticut array, a deployment of 15 broadband seismic stations across northern Connecticut. This linear array crosses a number of major terrane boundaries and traverses the Mesozoic Hartford Rift Basin in its central portion; its dense station spacing affords an opportunity to probe anisotropic structure on length scales that are relevant for the complex geology of southern New England. We find evidence for average fast splitting directions that are generally parallel to the absolute motion of the North American Plate, but in a few specific regions they are aligned with local tectonic boundaries. We document a striking decrease in splitting delay times (measured at low frequencies) from 0.9 s at the western end of the array to 0.2 s at the eastern end. We discuss several scenarios that might explain this observation, and explore the implications of our measurements for both present-day mantle flow and past lithospheric deformation beneath southern New England.

Plain Language Summary The U.S. state of Connecticut exhibits complicated bedrock geology that reflects a complex tectonic history. This includes a series of mountain-building events that formed the Appalachian Mountains and the Pangea supercontinent hundreds of millions of years ago, as well as the breakup of Pangea about 200 Myr ago. There is evidence for dynamic processes taking place in the upper mantle today beneath New England; these processes may play a role in shaping the surface topography and/or the deep structure of the tectonic plate. We use a set of seismic stations that were deployed across Connecticut to study seismic waves that have passed through the upper mantle beneath southern New England, traveling nearly vertically beneath the seismic stations. We measure how waves propagate differently in different directions (known as seismic anisotropy) and use these measurements to learn about how past tectonic events have affected the deep part of the plate, and how the upper mantle is flowing today beneath southern New England. We find evidence that there may be mantle upwelling (vertical flow) beneath the eastern portion of Connecticut today, and that the deep structure of the plate was altered by past tectonic events during the formation of the Appalachians.

1. Introduction

1.1. Tectonic Background

The bedrock geology of southern New England is extraordinary in its complexity, and reflects a range of plate tectonic processes, including subduction and terrane accretion during the Appalachian Orogeny and extension and rifting during the breakup of the Pangea supercontinent. Neoproterozoic rifting of Rodinia created the Laurentian passive margin preserved in western New England (Figure 1). Mesoproterozoic Grenvillian crust is exposed in the Green Mountain and Berkshire massifs in Vermont and Massachusetts (Karabinos and Aleinikoff, 1990; Karabinos et al., 2008; Ratcliffe & Zartman, 1976; Zen, 1983). Neoproterozoic to

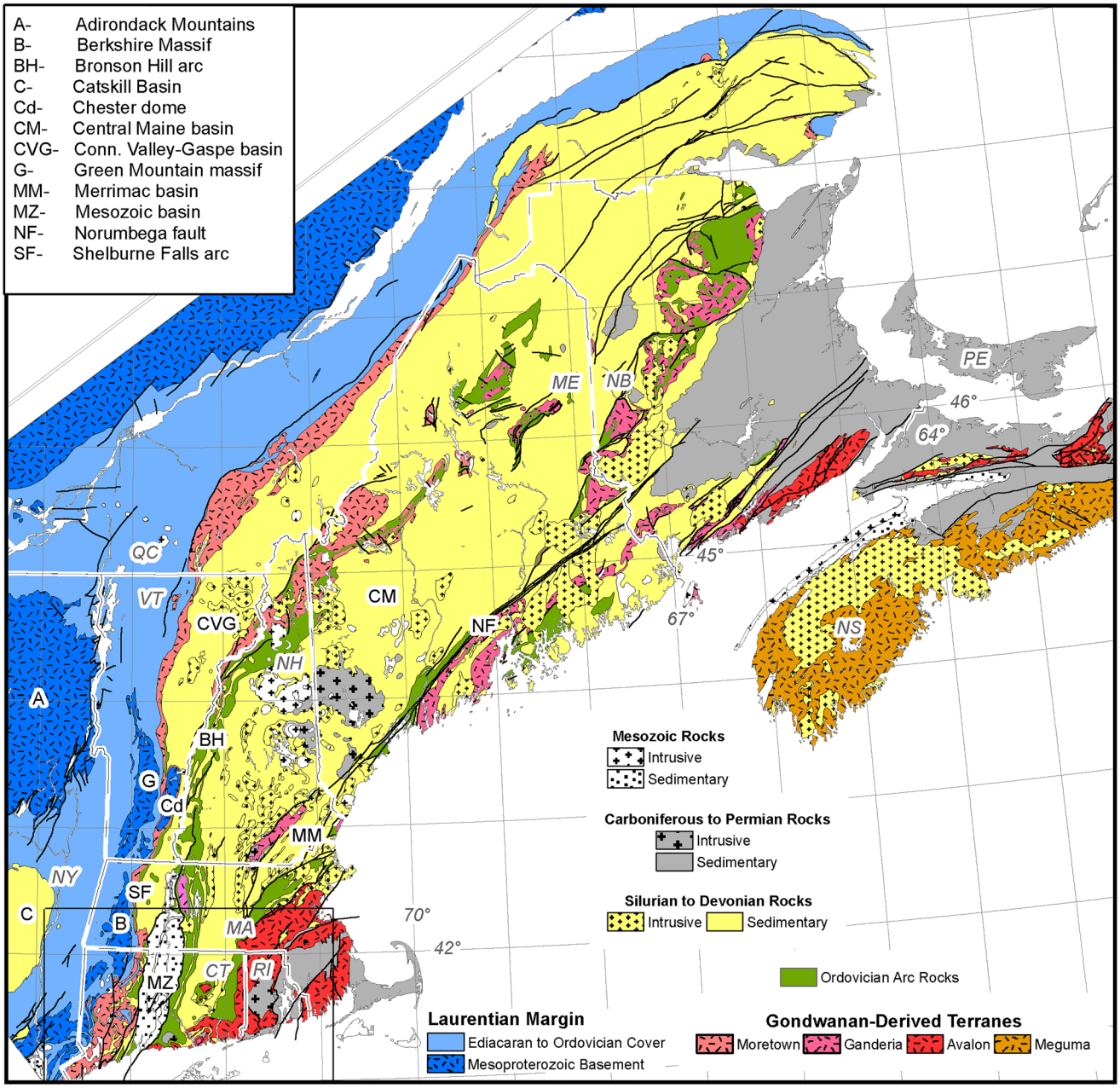

Figure 1. Tectonic map of the northern Appalachians, based on Hibbard et al. (2006) and Karabinos et al. (2017). Locations of U.S. states are shown with abbreviations in italics (Connecticut—CT; Massachusetts—MA; Rhode Island—RI; Vermont—VT; New Hampshire—NH; Maine—ME; New York—NY). Box at lower left shows the approximate area of the station map in Figure 2a.

Ordovician, rift to drift sediments were deposited on the Laurentian continental shelf and slope-rise (Karabinos et al., 2017; Macdonald et al., 2017; Stanley & Ratcliffe, 1985). Rocks east of the rifted margin in the New England Appalachians (Figure 1) were accreted to Laurentia during a succession of Paleozoic collisions with Gondwanan-derived microcontinents. Accretion of microcontinents and arcs ended when Laurentia and Gondwana collided to form Pangea during the Permian Alleghenian orogeny (Hatcher, 2010).

The onset, duration, and plate-tectonic geometry of the Paleozoic orogenies are widely debated, and what follows is a brief summary of tectonic events. The best-preserved evidence for plate tectonic geometry comes from the Ordovician Taconic orogen in western New England (Figure 1), which began approximately

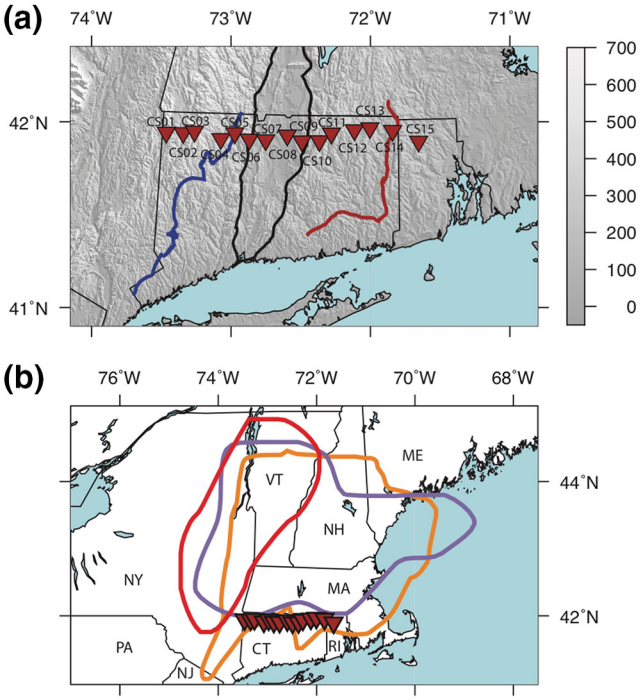

Figure 2. (a) Map of seismic stations used in this study. Background grayscale shows topography (as shown by scale at right, in m), triangles indicate station locations, and labels show station names. Thick lines indicate major tectonic boundaries (as shown in Figure 1), including the eastern edge of Laurentia (blue), the boundaries of the Mesozoic Hartford Basin (black), and the western edge of the Avalon terrane (red). (b) Different estimates of the boundary of the Northern Appalachian Anomaly at a depth of 200 km in the upper mantle, after Menke et al. (2016) and Levin et al. (2018). Red line indicates the 4.45 km/s shear velocity (V_S) contour in the model of Porter et al. (2016); purple line indicates the 3% slower than average V_S contour in the model of Schmandt and Lin (2014); orange line indicates the contour that is 0.06 km/s below the mean V_S from the model of Menke et al. (2016). Red triangles indicate SEISConn station locations. State names are marked with abbreviations: Connecticut—CT; Massachusetts—MA; Rhode Island—RI; Vermont—VT; New Hampshire—NH; Maine—ME; New York—NY; New Jersey—NJ; Pennsylvania—PA. SEISConn, Seismic Experiment for Imaging Structure Beneath Connecticut.

470 Ma when rocks of the Laurentian margin were subducted beneath the Moretown terrane (Karabinos et al., 2017; Macdonald et al., 2014). The Shelburne Falls magmatic arc formed on the Moretown terrane above an east-dipping subduction zone (Figure 1). Remnants of oceanic crust and mantle are commonly exposed along the suture between Laurentia and the Moretown terrane (Doll et al., 1961; Zen, 1983), and evidence for blueschist facies metamorphism is present in northern Vermont (Laird et al., 1984). Newly documented ultrahigh-pressure metamorphism from northern Vermont indicates that some Laurentian sediments were subducted to depths greater than 75 km (Gonzalez et al., 2020), suggesting that Laurentian crust was present, and may still exist at depth, far east of the current suture zone. The Bronson Hill magmatic arc may have also formed on the Moretown terrane, but above a west-dipping subduction zone that developed outboard of the newly accreted microcontinent (Karabinos et al., 2017; Macdonald et al., 2014). Slab breakoff of Laurentian lithosphere must have occurred before subduction polarity reversed, if this model is correct.

Ganderia, another Gondwanan-derived terrane, was accreted during the Late Ordovician to Early Silurian Salinic orogeny, which is better preserved in the Canadian Appalachians than it is in New England (van Staal et al., 2009). Avalonia collided during the Late Silurian to Middle Devonian Acadian orogeny (Bradley et al., 2000; Wintsch et al., 1992). Meguma, well preserved in Nova Scotia (Figure 1), was accreted during the Late Devonian Neoacadian orogeny (van Staal et al., 2009, 2012). Gondwana collided with Laurentia in the Permian during the final stage of the Appalachian orogenic cycle (Hatcher, 2010). Although the Alleghenian orogeny deformed rocks throughout the Central and Southern Appalachians, its effects in New England are limited to eastern Massachusetts, Rhode Island, and eastern Connecticut.

Early Mesozoic rifting of Pangea (Olsen, 1997) exploited lithospheric weaknesses in the Appalachian orogen and created the Atlantic passive margin and numerous failed rift basins (Withjack et al., 1998, 2003). The Hartford basin (Figure 1) in central Connecticut formed in response to extension and exposes Mesozoic sedimentary, volcanic, and shallow intrusive rocks (Olsen, 1997). The volcanic and intrusive units are part of the geographically extensive Central Atlantic Magmatic Province (CAMP; e.g., Marzoli et al., 1999), and their emplacement was likely associated with modification of lower crustal structure beneath the Hartford basin (Gao et al., 2020). Parts of New England have been affected by post-CAMP magmatic activity (e.g., Kinney et al., 2020), including the White Mountain Magma Series (WMMS) and Cretaceous magmatism in and around New Hampshire that may reflect the passage of the Great Meteor Hot Spot. Late Cretaceous accelerated exhumation in the White Mountains of New Hampshire has been proposed by Amidon et al. (2016). Pazzaglia and Brandon (1996) analyzed the offshore sedimentary record and suggested that asthenospheric flow-driven uplift during the Miocene created dynamic topography in the Northern Appalachians.

Both the post-CAMP volcanism and the pulses of accelerated exhumation during the Late Cretaceous (Amidon et al., 2016) and Miocene (Pazzaglia & Brandon, 1996) may be related to the present-day Northern Appalachian Anomaly (NAA; e.g., Menke et al., 2016; Schmandt & Lin, 2014). The NAA is a region of anomalously slow upper mantle velocities, centered beneath New Hampshire and perhaps extending as far south as northern Connecticut (Figure 2), that is clearly delineated in a number of recent tomographic models (e.g., Golos et al., 2018; Porter et al., 2016; Savage et al., 2017; Schmandt & Lin, 2014). Dong and Menke (2017) found evidence for high seismic attenuation in the NAA, and there is some evidence for

locally high heat flow based on temperature measurements at thermal springs (Menke et al., 2018). Levin et al. (2018) documented a region of weak or absent shear wave splitting in the vicinity of the NAA, indicating weak upper mantle anisotropy, and suggested that this reflects localized mantle upwelling.

While the basic framework of Paleozoic orogenesis, Mesozoic rifting and supercontinental breakup, post-rifting modification of the margin through magmatism and accelerated exhumation, and possible present-day dynamic processes in the upper mantle beneath New England has been sketched out, a number of major unsolved problems remain. Outstanding questions that are relevant to this study include how the lithosphere was deformed during this series of tectonic events, and to what extent the present-day structure and fabric of the lithosphere can shed light on the nature and geometry of past episodes of orogenesis and rifting. Furthermore, the precise nature of present-day mantle flow beneath New England remains enigmatic. Is flow in the asthenospheric upper mantle dominated by plate-motion-parallel shearing, as has been suggested by some previous investigations (e.g., Long et al., 2016; Yang et al., 2017)? How spatially extensive is the zone of vertical upwelling flow suggested by Levin et al. (2018), and how far south does it extend? This paper aims to address these unanswered questions through the measurement of SK(K)S splitting due to upper mantle seismic anisotropy beneath southern New England.

1.2. Seismic Anisotropy and Mantle Deformation Beneath the Appalachians

Observations of seismic anisotropy, the dependence of seismic wave speeds on wave propagation direction or polarization, are a powerful tool for understanding upper mantle deformation and for testing the predictions of tectonic models (e.g., Silver, 1996). This is because when mantle rocks are deformed under dislocation creep conditions, they form crystallographic or lattice preferred orientation (CPO or LPO), leading to a bulk seismic anisotropy of the aggregate (e.g., Karato et al., 2008; Skemer & Hansen, 2016). Seismic anisotropy can also occur as a result of shape preferred orientation (SPO) of materials with elastic properties that contrast with those of the matrix, although this mechanism is thought to be less relevant than CPO for most regions of the upper mantle (e.g., Skemer & Hansen, 2016). Observations of shear wave splitting or birefringence are a common tool for characterizing upper mantle anisotropy (e.g., Long & Silver, 2009; Silver, 1996). When a seismic phase such as SKS passes through an anisotropic region, it splits into fast and slow components; the polarization of the fast quasi-S wave reflects the geometry of anisotropy, and the time delay between the fast and slow components reflects a combination of the strength of anisotropy and the path length through the anisotropic region. While SKS splitting measurements are a powerful and commonly used tool for characterizing anisotropy, a major limitation is that they lack depth resolution, because shear wave splitting is a path-integrated signal (in the case of SKS waves, from the core-mantle boundary to the surface). Therefore, a major challenge with the interpretation of SKS splitting data sets, particularly in continental regions, is separating the signal due to anisotropy in the lithosphere (which reflects frozen-in deformation from past tectonic processes) from that due to anisotropy in the asthenosphere (which reflects present-day mantle flow). Lithospheric anisotropy may encompass contributions from both the mantle lithosphere and from the crust. While the contribution to SKS splitting from anisotropy within the crust is generally thought to be small in continental regions (generally ~0.1 s; Barruol & Mainprice, 1993; Silver, 1996), it may represent a significant portion of the signal in regions where the overall delay times are modest.

SKS splitting has been extensively studied beneath the Appalachians, including with data sets from the pre-USArray era (e.g., Barruol et al., 1997; Levin et al., 1999; Long et al., 2010; Wagner et al., 2012). Measurements from the USArray Transportable Array (TA), which covered the continental United States with ~70 km station spacing, have revealed complex patterns of SKS splitting beneath the eastern U.S. (e.g., Long et al., 2016; Yang et al., 2017). These have been variously interpreted as mainly reflecting anisotropy in the asthenosphere (e.g., Yang et al., 2017), in the lithosphere (e.g., White-Gaynor & Nyblade, 2017), or a combination of both (e.g., Long et al., 2016). Beneath New England, previous studies (Li et al., 2019; Long et al., 2016; Yang et al., 2017) have documented fast splitting directions that generally trend nearly E-W, close to the direction of absolute plate motion (APM) of the North American Plate, but oblique or perpendicular to geologic structures, which tend to strike N-S (Figure 1). In other regions of the Appalachians, including the central and southern Appalachians (e.g., Long et al., 2016; Wagner et al., 2012) and beneath Newfoundland in eastern Canada (e.g., Gilligan

et al., 2016), fast directions appear to relate more to tectonic features, such as the strike of Appalachian Mountains topography or local terrane boundaries.

Adding to the body of literature on SKS splitting based on TA data, several recent studies have sought to exploit the information contained in long-running seismic stations, which typically yield superior directional coverage and much larger data sets than temporary stations. For example, Levin et al. (2018) examined data from New England and found evidence for a number of stations that were dominated by SKS arrivals that exhibited weak or absent splitting, indicating weak upper mantle anisotropy. Levin et al. (2018) proposed that this zone of weak SKS splitting, which seems to correspond with the NAA in the upper mantle, reflects mainly vertical mantle flow. Li et al. (2019) examined long-running seismic stations throughout the northeast U.S. and found evidence for regionalized anisotropic domains that exhibit coherent splitting behavior; they proposed that lateral changes in lithospheric anisotropy, perhaps in combination with changes in present-day mantle flow, may explain the occurrence of these domains.

Another recent innovation in the study of upper mantle anisotropy beneath the eastern U.S. has been the advent of data sets from arrays that feature dense station spacing, allowing for the sampling of the mantle lithosphere over the short length scales that are relevant for geologic structures. For example, Aragon et al. (2017) presented SKS splitting observations for the dense MAGIC array in the central Appalachians, and showed a sharp transition in splitting behavior across the Appalachian Mountains, which they attributed to a change in lithospheric anisotropy. Similarly, Chen et al. (2018) measured SKS splitting across the dense QMIII array in the northern Appalachians, documenting a lateral change in splitting delay times that corresponds to the edge of cratonic lithosphere at depth. These studies and others (e.g., Diaz et al., 2010; Polet & Kanamori, 2002; Rümpker et al., 2003; Ryberg et al., 2005) have demonstrated the power of data from closely spaced stations in documenting and interpreting lateral changes in upper mantle seismic anisotropy on relatively short length scales, allowing not only for a more detailed picture of upper mantle structure, but also for thorough comparisons between shear wave splitting behavior and geologic architecture that enables a more informed view of underlying tectonic processes.

1.3. The SEISConn Array

The Seismic Experiment for Imaging Structure Beneath Connecticut (SEISConn; Gao et al., 2020; Long & Aragon, 2020) was a deployment of 15 seismic stations across northern Connecticut and Rhode Island (Figure 2). SEISConn was designed as a high-density array, with an average interstation distance of ~10 km, and it enables the characterization of variations in shear wave splitting over short length scales beneath northern Connecticut, and the interrogation of the possible spatial relationships between anisotropy in the mantle lithosphere and major geologic and tectonic boundaries. The SEISConn array traversed a number of such boundaries, including the eastern boundary of Laurentia (blue line in Figure 2a) in the western portion of the array, the Mesozoic Hartford Basin in the central portion of the state (bounded by black lines), and the western edge of the Avalon terrane in the eastern part of the array (red line). This allows us to investigate whether these boundaries are associated with transitions in shear wave splitting behavior, and may illuminate the nature of past lithospheric deformation due to fundamental tectonic processes such as subduction, terrane accretion, and rifting.

1.4. Goals of This Study and Hypothesis Testing

We will evaluate SKS splitting measurements at SEISConn stations against predictions made by four different hypotheses that may explain upper mantle anisotropy beneath the region. The first hypothesis is that upper mantle anisotropy beneath Connecticut is controlled by buoyant upwelling associated with the NAA (Figure 2). This scenario is based on the model proposed by Levin et al. (2018), who documented weak SKS splitting within the NAA to the north of the SEISConn array. If the region dominated by mantle upwelling extends as far south as northern Connecticut, then we may expect to see weak or absent SKS splitting beneath (all or part) of the SEISConn array. The second hypothesis is that upper mantle anisotropy is controlled by ongoing shear in the asthenospheric upper mantle driven by the absolute motion of the North American plate. In this scenario, we would expect to see relatively uniform SKS splitting across the

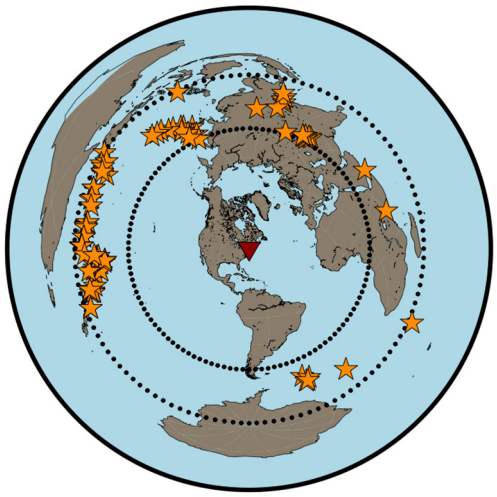

Figure 3. Map of earthquakes (stars) used in this study that yielded at least one usable splitting measurement. The center of the SEISConn array is shown with a triangle. Dotted lines indicate epicentral distance bounds of 90° and 130°, which were used for event selection (although we did use one event that was slightly beyond the 130° cutoff). SEISConn, Seismic Experiment for Imaging Structure Beneath Connecticut.

SEISConn array, with fast directions that are nearly parallel to APM and little variability in delay times. A third hypothesis is that upper mantle anisotropy primarily reflects frozen-in structure in the lithosphere from past tectonic deformation, potentially including the various phases of Appalachian orogenesis and subsequent extension and rifting. If this were the case, we would expect to observe fast splitting directions that correlate with geologic and tectonic structures, and/or that change abruptly across major boundaries (e.g., the edges of Laurentia, Avalonia, or the Hartford Basin). A fourth and last hypothesis is that both asthenospheric and lithospheric anisotropy are present, each making a significant contribution to SKS splitting. In this case, we would expect to see complexity in SKS splitting behavior, including variations in apparent splitting with the direction or frequency content of the incoming waves.

Keeping in mind this set of hypotheses whose predictions can be tested, our study has several specific goals. We aim to characterize SKS splitting behavior beneath northern Connecticut in detail, including the possible presence of backazimuthal variations and/or frequency dependence in apparent splitting. Exploiting the dense station spacing of the SEISConn array, we wish to document any small-scale variations in splitting behavior and understand the relationships between these variations and geologic structures. We aim to discover whether the region of weak SKS splitting associated with the NAA by Levin et al. (2018) extends as far south as northern Connecticut, and if so, what that tells us about the dynamics and evolution of the NAA. Our study region cuts across a boundary between two of the regional anisotropic domains of the northeastern U.S. documented by Li et al. (2019), so we are in a position to define this boundary more precisely and understand in detail how SKS splitting changes across it. A crucial question is whether SKS splitting beneath southern New England is controlled by anisotropy in the asthenosphere, in the lithosphere, or a combination of the two. The relative contributions will be evaluated by examining our data for the presence of variability in apparent splitting with backazimuth and/or frequency, which can indicate multiple layers of anisotropy, and through careful comparisons between our measurements and indicators such as APM and geologic structures.

2. Data and Methods

2.1. Data, Event Selection, and Preprocessing

We used data from the broadband SEISConn array (Long & Aragon, 2020; Figure 2). Data collection for SEISConn began in August 2015 and ended in August 2019. The seismic stations employed Trillium 120 PA broadband sensors and Taurus digitizers, owned and operated by Yale University. The 15 stations were closely spaced, the average being ~10 km apart (compared to the ~70 km nominal spacing of the TA), and individual stations recorded between 18 and 47 months of data. SEISConn data were retrieved from the archive of the Incorporated Research Institutions for Seismology (IRIS) Data Management Center (DMC).

We used SplitRacer, a Matlab-based graphical interface tool for shear wave splitting analysis (Reiss & Rümpker, 2017), for data preprocessing and splitting measurements. Processing steps in SplitRacer include data download, initial screening and categorizing of waveforms, filtering, particle motion analysis, and splitting analysis for selected SK(K)S waveforms using multiple measurement methods. We selected 802 candidate earthquakes of moment magnitude 6.0 and greater at epicentral distances between 90° and 130° between August 2015 and August 2019 for initial analysis. Of these, 93 events yielded at least one usable splitting measurement (Figure 3). As with many SK(K)S splitting studies, azimuthal coverage in our study is imperfect, with most events located in Tonga and other western Pacific subduction zones. We identified high-quality SKS and SKKS waveforms for analysis through both automated and visual checking for high signal-to-noise ratio, good waveform clarity, and measured initial polarizations within 10° of the backazimuth (that

is, the station-to-event azimuth; because SKS polarizations are controlled by a P-to-SV conversion at the core-mantle boundary, the initial polarizations should correspond to the backazimuth).

We measured splitting of SKS and SKKS phases over a range of frequencies, following previous work by Eakin and Long (2013), with the goal of characterizing any frequency dependence in apparent splitting. Because data at different frequencies are sensitive to different volumes of mantle structure (e.g., Favier and Chevrot, 2003; Long et al., 2008; Mondal & Long, 2019; Sieminski et al., 2008), frequency-dependent splitting observations generally indicate laterally and/or vertically complex anisotropic structure. We applied three different bandpass filters to the data, retaining energy at periods from 8 to 25 s, 5 to 8 s, and 1 to 5 s. We refer to these as the low-frequency, medium-frequency, and high-frequency filters, respectively. Previous studies have identified frequency-dependent shear wave splitting in a variety of settings, using either SKS waves (e.g., Eakin & Long, 2013; Long, 2010) direct S waves (e.g., Wirth & Long, 2010), or a combination of phases (e.g., Marson-Pidgeon & Savage, 1997). Because high-frequency data are often more sensitive to shallow anisotropic structure, measurements at high frequencies can potentially illuminate lithospheric contributions to splitting better than lower-frequency data.

2.2. Shear Wave Splitting Measurements: Methods and Examples

We used two different measurement methods, each of which is implemented in SplitRacer: the transverse component minimization (TCM) method of Silver and Chan (1991) and the multichannel method of Chevrot (2000). The TCM method estimates the splitting parameters (fast polarization direction, ϕ, and delay time, δt) from individual waveforms by grid-searching over all possible combinations of (ϕ, δt) to best minimize the transverse component energy on the corrected waveforms (and thus remove the effect of splitting). The multichannel method measures a quantity known as splitting intensity, which is derived from the amplitude ratio between the transverse component and the time derivative of the radial component, on individual SK(K)S waveforms. A set of splitting intensity measurements at an individual station are interpreted collectively by plotting the splitting intensities as a function of backazimuth (known as the splitting vector) and fitting a $\sin 2\theta$ curve to them; the phase and amplitude of the sinusoid indicate the fast direction and delay time, respectively. The multichannel method relies on the principle that the transverse component energy varies with the initial polarization of the wave (equivalent to the backazimuth for SK(K)S waves), such that the energy is zero when the wave is polarized parallel or perpendicular to the fast axis of the anisotropic medium, and maximized when the polarization direction is 45° from a symmetry axis.

Each of the analysis methods we employ has strengths and weaknesses (e.g., Long & Silver, 2009; Monteiller & Chevrot, 2010), and they are particularly powerful in combination. The TCM method has the advantage of providing an estimate of splitting parameters for each individual waveform, offering the opportunity to investigate possible variations in apparent splitting as a function of backazimuth; such variability is an indicator of complex anisotropy (multiple anisotropic layers and/or small-scale lateral variability in structure). However, individual TCM measurements are less robust than splitting intensity measurements, particularly for the case of "near-null" splitting, in which the amount of transverse component energy is small. Furthermore, the TCM method is poor at measuring weak splitting (small delay times); for example, at low frequencies (periods greater than ~8 s), the TCM cannot detect splitting with delay times less than ~0.5 s (e.g., Long & Silver, 2009). The multichannel method has the advantage that individual splitting intensity measurements are more robust and plentiful than individual TCM measurements, and the method can easily measure splitting intensity for the "near-null" case of weak transverse component energy. However, a major drawback of the multichannel method is that because the splitting intensity is commutative (e.g., Chevrot, 2006; Silver & Long, 2011) and can be summed along the raypath, the method cannot easily diagnose the presence of multiple anisotropic layers. In this case, the splitting vector takes the form of a sinusoid whose phase and amplitude represent the sum of sinusoids associated with the individual layers; it cannot be easily distinguished from a sinusoid that results from a single layer of anisotropy.

We applied both measurement methods to SK(K)S phases measured at SEISConn stations, implementing a number of quality control procedures for each measurement. For the TCM method, we

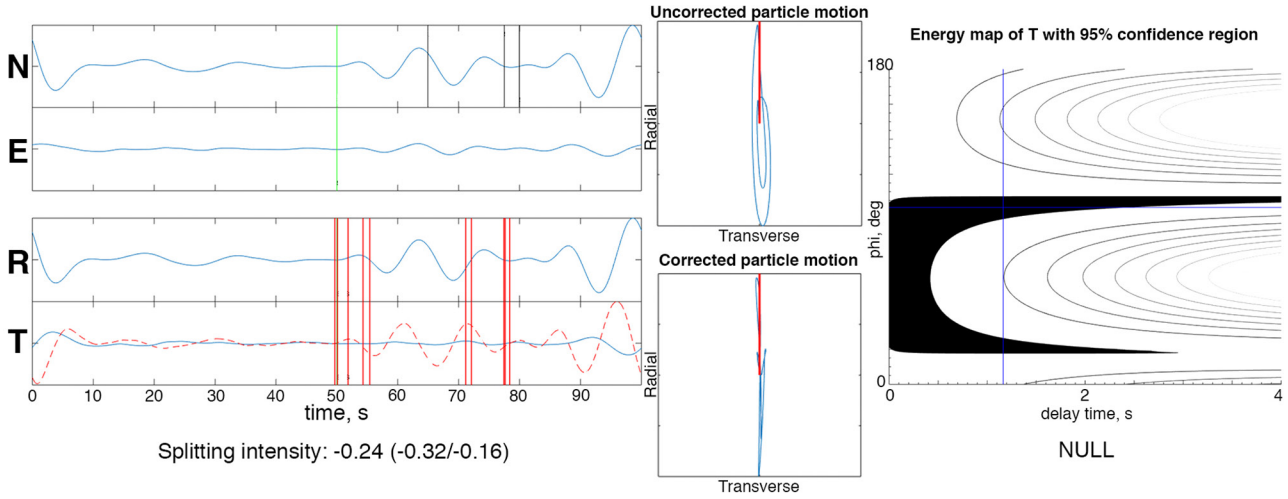

Figure 4. Example of a high-quality ("good") null measurement, made at station CS08 for an earthquake on August 8, 2017 at an epicentral distance of 92° and a backazimuth of 17°. Data were preprocessed using the low-frequency filter. Horizontal component waveforms (blue lines) are shown at left, viewed both as north (N)/east (E) and radial (R)/transverse (T) components. The T component plot also shows the time derivative of the R component (dashed red line). Expected arrival time for the SKS phase is shown with a green vertical line; theoretical arrival times for other phases (which do not actually appear on the seismogram) are shown with short black vertical lines on the N trace. Vertical red lines on the R and T traces show a selection of windows used to compute splitting parameters, as described in Reiss and Rümpker (2017). Center panels show uncorrected (top) and corrected (bottom) particle motions (blue lines), with the red lines indicating the event backazimuth (aligned along the radial direction). Corrected particle motion is based on the best fitting pair of splitting parameters (ϕ, δt) calculated using the transverse component minimization method. Right panel shows a map of transverse component energy for different candidate values of the splitting parameters (ϕ, δt), with the 95% confidence region shown in black. Estimated splitting intensity values (with 95% error estimates) for this waveform are shown at lower left; because this is a null arrival, estimated (ϕ, δt) values are not well constrained.

visually evaluated the linearity of the corrected SK(K)S wave's particle motion, and (for non-null measurements) we checked to be sure that the amplitude of the transverse component in the measurement was above the transverse component noise level before the SK(K)S arrival (to avoid interpreting transverse component noise as splitting). We assigned a quality ranking of "good," "average," or (in a few cases) "poor" to each non-null measurement, based on the size of the 95% confidence region and the quality of the corrected waveforms. While the choice of criteria for quality rankings in shear wave splitting studies is always somewhat subjective, we chose criteria that were similar to those used in previous studies using comparable approaches (e.g., Aragon et al., 2017; Long et al., 2016). "Good" measurements had 95% confidence regions of up to approximately ±25° in ϕ and ±0.6 s in δt, while "average" measurements were up to approximately ±35° in ϕ and ±1.0 s in δt. We note that SplitRacer implements the corrected error estimates for the TCM method proposed by Walsh et al. (2013), so the error bars are larger than, and not directly comparable to, those calculated in many previous studies using other software. In a few cases, we included measurements with even larger error bars, provided that the waveforms were clear, the measurements were stable over a range of randomly selected measurement windows (Reiss & Rümpker, 2017), and the corrected particle motion was nearly perfectly linear. We included these measurements (6 total, all at low or medium frequency) in our maps and interpretation; we caution that they are more uncertain than the bulk of the measurements, but we emphasize that none of our interpretations hinge solely on "poor" quality measurements. For the multichannel method, the quality control procedure was simpler; we did not assign a quality rating, as the estimate of the splitting intensity and its 95% confidence region is quite straightforward (Chevrot, 2000). However, we did visually check the waveforms to be sure that the transverse component wave shape matched the shape of the time derivative of the radial component. Example waveforms and diagnostic plots for a typical null measurement (measured at low frequency) are shown in Figure 4, and similar plots for a typical split measurement (of average quality, measured at medium frequency) are shown in Figure 5.

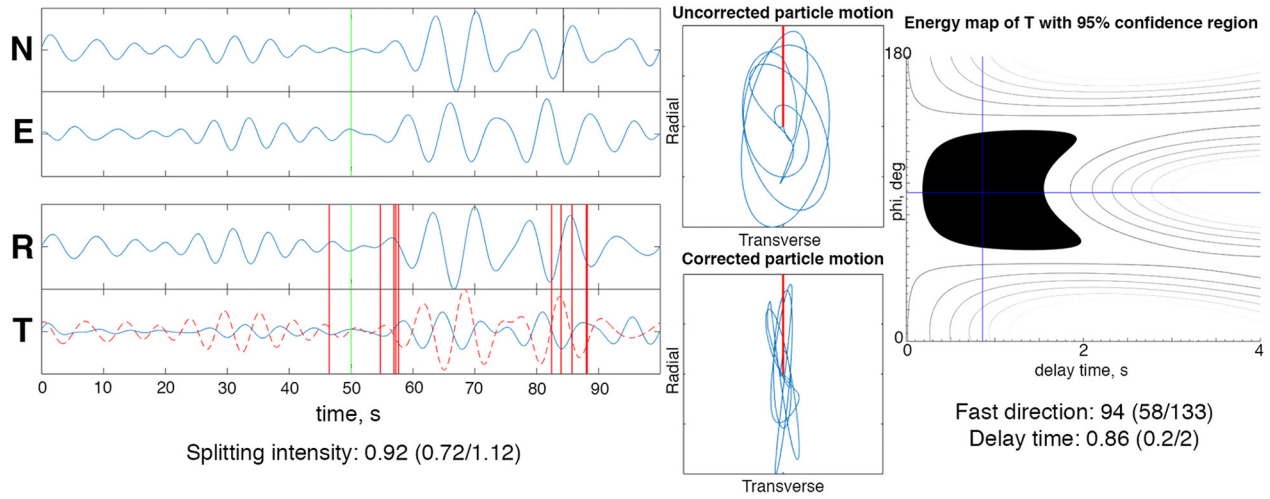

Figure 5. Example of a medium quality ("average") non-null measurement. Measurement was made at station CS03 for an earthquake on July 29, 2016 at an epicentral distance of 110° and a backazimuth of 321°. Data were preprocessed using the medium-frequency filter. Plotting conventions are as in Figure 4. Estimated splitting intensity values (with 95% error estimates) are shown at lower left, and estimated splitting parameters (ϕ, δt) derived from the transverse component minimization method, along with 95% error estimates, are shown at lower right.

3. Results

3.1. Transverse Component Minimization Results

We obtained a total of 213 individual TCM results at SEISConn stations across the three frequency bands. Specifically, we obtained 142 measurements using the low-frequency filter, 56 using the medium-frequency filter, and 15 using the high-frequency filter. Most (87%) measurements were made on SKS phases, while a minority (13%) were made on SKKS phases. The data set is dominated by null SK(K)S arrivals, particularly at low frequencies; nearly all (97%) of the low-frequency measurements were null, along with 50% of the medium-frequency measurements and 27% of the high-frequency measurements. Most of the non-null measurements were of "average" quality, with a few (8) rated "good" and a small number (3) rated "poor." A table of individual measurements, including event and station information and error estimates, can be found in the online Table S1.

All TCM measurements are shown in Figure 6, which displays stereographic plots (in which measurements are plotted as a function of backazimuth and incidence angle) for each SEISConn station. These plots reveal evidence for complex and laterally variable shear wave splitting beneath southern New England. While the backazimuthal coverage is decidedly imperfect, we observe some evidence for apparent splitting that varies with backazimuth at several stations, particularly in the western portion of the array (stations CS01-CS05). While many of the observed fast directions trend roughly E-W, there are notable exceptions at a few stations, particularly CS06 (which is mostly dominated by null arrivals, but which has one non-null measurement with a nearly N-S fast direction) and CS15 (which has a cluster of well-constrained splitting measurements from waves arriving from the west that all display N-S fast directions). There is a group of stations in the central portion of the array (CS09-CS12) that is dominated entirely by null arrivals or very small delay times. Splitting across the SEISConn array is generally fairly weak, with many measured delay times less than 0.5 s, particularly in the eastern portion of the array, and clear observations of null SK(K)S arrivals across a large swath of backazimuths at many stations.

3.2. Multichannel Method Results

We obtained a total of 555 individual splitting intensity results (including both SKS and SKKS) at SEISConn stations across the three frequency bands, contained in Table S2. Specifically, we obtained 330 measurements using the low-frequency filter, 191 using the medium-frequency filter, and 34 using the high-frequency filter.

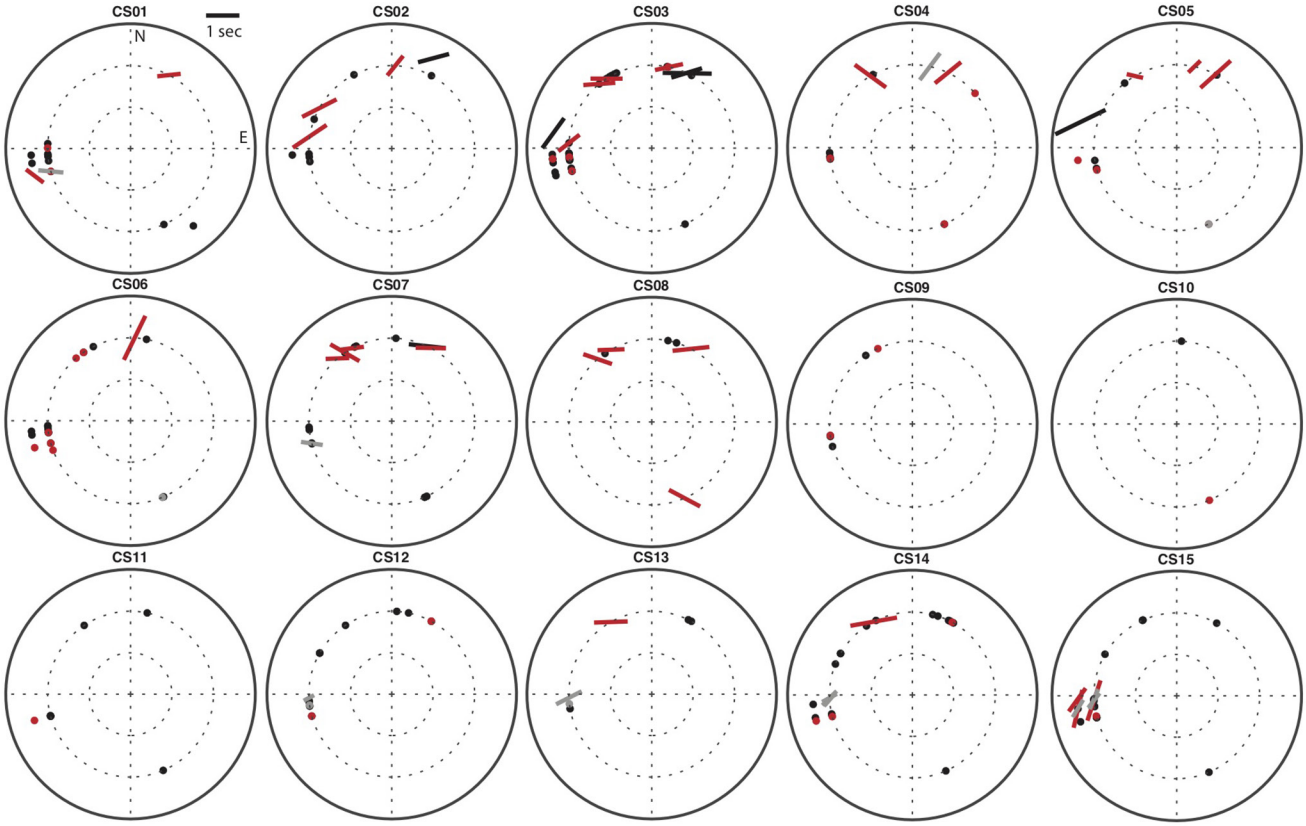

Figure 6. Stereographic plots of individual splitting measurements made at each station (station names at top) using the transverse component minimization measurement method, across all frequency bands. Measurements are plotted according to the event backazimuth (degrees from north, as shown in the upper left) and the incidence angle (distance from the center of the plot), which we assume to be 10° for SKS phases and 12° for SKKS phases. Null measurements are indicated with circles; non-null measurements are indicated with bars, with the orientation of the bar corresponding to the fast splitting direction and the length of the bar corresponding to the delay time, as shown by the scale bar at upper left. Symbol colors indicate the frequency range, with low-frequency measurements in black, medium-frequency measurements in red, and high-frequency measurements in gray.

This yields an average of 12–22 measurements per station using the low- and medium-frequency filters. The relatively small number of well-constrained measurements at high frequencies precluded further analysis of the splitting intensity measurements in this frequency band, and was likely a consequence of a departure from the assumption (made by the multichannel method) that the transverse component waveform takes the shape of the radial component derivative. This assumption is only valid for cases in which the splitting delay time is much smaller than the dominant period of the wave, and may be violated at high frequencies (periods between 1 and 5 s in our study).

Of the 555 splitting intensity measurements we obtained, 156 were part of an SKS-SKKS pair (that is, measurements of SKS and SKKS phases for the same event at the same station). Such SKS-SKKS pairs are useful for evaluating whether there may be a contribution to splitting from seismic anisotropy in the lower mantle. Because SKS and SKKS have similar raypaths in the upper mantle, but diverge significantly in the lowermost mantle, an observation of discrepant splitting between SKS and SKKS phases from the same event (measured on the same seismogram) suggests a contribution from the deep mantle to one or both phases (e.g., Deng et al., 2017; Reiss et al., 2019). SKS-SKKS splitting discrepancies have been previously documented beneath North America (e.g., Asplet et al., 2020; Lei & Wen, 2020; Lutz et al., 2020), although these studies have also shown that seismic anisotropy in the upper mantle, not the lower mantle, represents the primary contribution to SK(K)S splitting observations. Of the 78 SKS-SKKS pairs we measured, a minority (18%) showed discrepancies between SKS and SKKS splitting intensity measurements (such that the 95% confidence regions for the measurements did not overlap). A small minority (7 out of 78, or 9%) showed strong discrepancies (splitting intensity differences greater than 0.4 s, with no overlap of 95% confidence

regions), suggesting a contribution from the lowermost mantle (e.g., Deng et al., 2017; Lutz et al., 2020; Reiss et al., 2019). Our identification of a few strongly discrepant SKS-SKKS phases at SEISConn stations warrants future study to explore whether SKS-SKKS splitting intensity discrepancies are widespread beneath New England. However, because only a small minority of SKS-SKKS pairs show evidence of a contribution from lowermost mantle anisotropy, we conclude that we can interpret our measurements as mainly reflecting upper mantle anisotropy beneath the SEISConn array.

For the low- and medium-frequency results, we fit a series of $\sin 2\theta$ curves to the splitting intensity data to obtain single-station average estimated splitting parameters (ϕ, δt). Splitting intensity (SI) is related to these parameters via the relation $\mathrm{SI} = -\delta t \sin 2\beta$, where β is the angle between the incoming polarization direction (equivalent to the backazimuth for SK(K)S waves) and the fast splitting direction ϕ (Chevrot, 2000). Splitting intensity data and $\sin 2\theta$ fits for all stations are shown in Figure 7. The observations are generally very well fit by $\sin 2\theta$ curves at all stations, although there are some outlier observations in the dataset (perhaps due to localized contributions from lowermost mantle anisotropy), and we must keep in mind that the backazimuthal coverage is imperfect. At a few stations, we did not have a sufficient number of observations to fit a sinusoidal curve to the data (CS02, CS09, CS10, and CS11 at medium frequencies; CS10 at low frequencies). The average splitting parameters derived for each station using the multichannel method are shown in Table S3.

Figure 7 demonstrates some striking spatial trends in the multichannel method results; most notably, we document a steady decrease in best fitting average delay times (derived from amplitude of the sinusoids) from west (CS01) to east (CS15) in the low-frequency data. Delay time values decrease steadily, nearly monotonically, from 0.9 s at the western end of the array to 0.2 s at the eastern end. Delay times measured at medium frequencies are also generally higher in the western part of the array than in the east, although a steady decrease is not observed at medium frequencies (as it is at low frequencies). At some individual stations (e.g., CS01, CS03, CS04, CS07, CS12), there is clear consistency between the low- and medium-frequency data, while at others (e.g., CS05, CS06, CS08, CS13, CS15) the sinusoidal fits are noticeably different. Given the relatively modest number of medium-frequency measurements, however, it is unclear how statistically different the sinusoidal fits really are at most of these stations. Only two stations (CS08 and CS15) seem to exhibit distinguishably different splitting behavior at low versus medium frequencies. The difference is particularly striking at CS15, where the medium frequency data exhibit higher splitting intensity values (and thus a larger average δt) than the low frequency data. The estimated ϕ values (derived from phase of the sinusoids) generally exhibit only slight variation across the array. At low frequencies, we document nearly E-W fast directions (average values of ~73°, equivalent to 253°) at stations in the western part of the array (CS01-CS07), which is very close to the APM direction of 250° (Gripp & Gordon, 2002) in a Pacific hotspot reference frame. Towards the central and eastern end of the array, there is a subtle counterclockwise rotation in ϕ. Trends are generally similar for the medium-frequency data, although there is more scatter. At medium frequencies, the counterclockwise rotation at the easternmost station (CS15) is particularly pronounced, with an estimated ϕ value of 56°.

The generally low δt values estimated from the splitting intensity data shed light on our finding of a very high proportion of nulls in the TCM dataset at medium and (particularly) low frequencies. At low frequencies, the δt values from the multichannel method range from 0.2–0.9 s; this range is below the average delay time value of 1 s in continental regions (e.g., Long & Silver, 2009; Silver, 1996) and smaller than the average SKS splitting delay times throughout eastern North America (e.g., Long et al., 2016; Yang et al., 2017). Because the TCM method cannot accurately measure weak splitting at low frequencies, and split waveforms with delay times less than ~0.5 s may be classified as null arrivals, this helps to explain the very large proportion of nulls in our TCM data set; the splitting is simply weak enough that many SK(K)S arrivals exhibit null splitting, particularly at low frequencies.

3.3. Shear Wave Splitting Across Connecticut in a Geologic and Tectonic Context

To put our results in a geologic and tectonic context, we show in Figures 8 and 9 maps of our splitting results on top of the bedrock geologic structure (as shown in Figure 1). The individual TCM measurements at medium and high frequencies (Figure 8) show considerable scatter, some of it undoubtedly related to complexities in splitting patterns (that is, backazimuthal variability) at individual stations. Still, a few

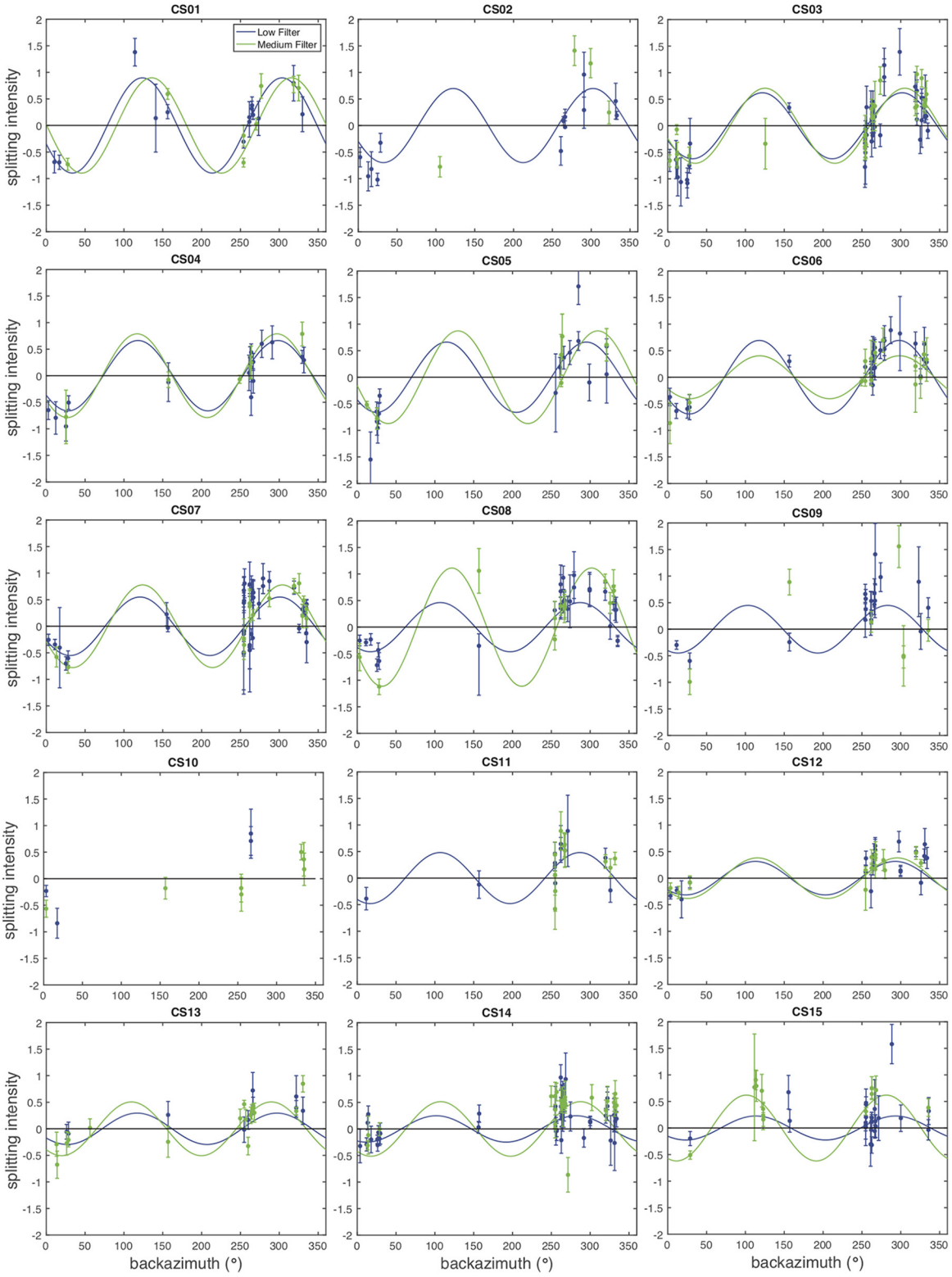

Figure 7. Results from the multichannel method at SEISConn stations, with station names at top. We show individual splitting intensity measurements (dots) with 95% confidence regions (error bars) in two different frequency bands (low-frequency filter in blue and medium-frequency filter in green, as indicated by the legend at top left). In most cases, sufficient backazimuthal coverage is available to fit a sin(2θ) curve to the data (blue curves for low-frequency measurements and green curves for high-frequency measurements) and retrieve the average splitting parameters (ϕ, δt) from the phase and amplitude of the curve, respectively. In cases where backazimuthal coverage is insufficient, no sin(2θ) curve is shown. SEISConn, Seismic Experiment for Imaging Structure Beneath Connecticut.

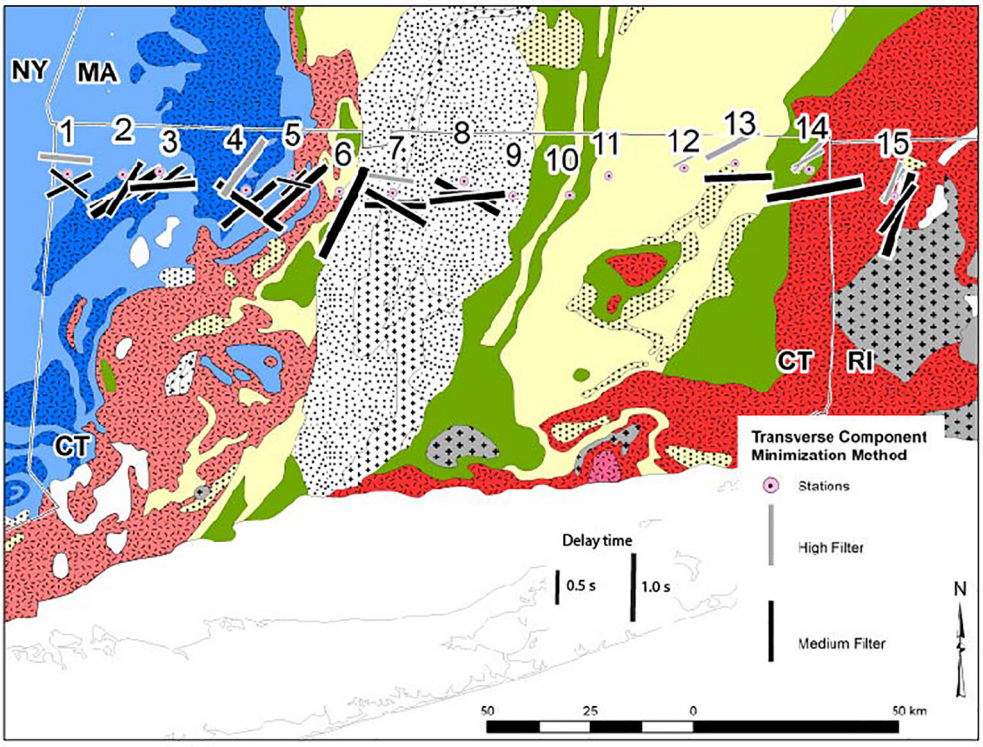

Figure 8. Map of individual non-null splitting measurements, derived from the transverse component minimization method, plotted on top of bedrock geologic units (symbols are as in Figure 1). Thin black lines indicate state boundaries, with state abbreviations shown. Stations are shown with red circles. We show measurements made using the medium-frequency filter (black bars; offset slightly to the south of the stations to show detail) and the high-frequency filter (gray bars; offset slightly to the north of the stations). (Low-frequency measurements are almost entirely dominated by null arrivals, so they are not shown.) Fast splitting orientations are indicated by the orientation of each bar; delay times are indicated by the length (and thickness) of each bar, as shown at the bottom of the figure. Delay times range from a minimum of 0.35 s (at station CS12) to a maximum of 1.5 s (at station CS06).

trends are evident. The generally E-W fast directions observed across much of the array clearly cut across the generally N-S trend of many of the geologic structures, as has been noted elsewhere in New England (e.g., Li et al., 2019; Long et al., 2016). However, there are a few specific examples where the local apparent fast directions seem to correlate with geologic boundaries. At stations CS04 and CS05, located close to the eastern extent of Laurentia (blue units in Figures 1 and 8), we see a subset of TCM fast directions (at both medium and high frequencies) oriented nearly NE-SW, in contrast to the more nearly E-W fast directions that dominate through much of the array. At station CS06, located close to the western boundary of the Hartford Rift Basin, there is a single non-null measurement (of "average" quality) that is aligned nearly N-S, similar to the structural trend of the basin itself. While we cannot place too much emphasis on a single measurement, it is well-constrained, with relatively small error bars on the fast direction estimate (26°, with the 95% confidence region ranging from 13° to 40°). At the easternmost station (CS15), which is the only station in the array located on the Avalon terrane, we obtained several well-constrained ϕ measurements that trend nearly N-S (at both medium and high frequencies, and mostly of "average" to "good" quality). This direction is parallel to the strike of the boundary between the Avalon terrane (to the east) and the Putnam-Nashoba belt on the trailing edge of Ganderia (to the west); the boundary itself is located roughly 10 km to the west of CS15 (close to the location of neighboring station CS14).

In order to visualize the geographic patterns in the TCM measurements more clearly, we divided the stations up into three geographic groups (western, stations CS01-CS06; Hartford Basin, stations CS07-CS09; eastern, stations CS10-CS15) and plotted histograms of individual ϕ and δt values (for both the medium- and high-frequency datasets combined) within each group (Figure 10). We focused on the medium-frequency band, since this band had the largest number of (non-null) measurements, although the relatively small number of meas-

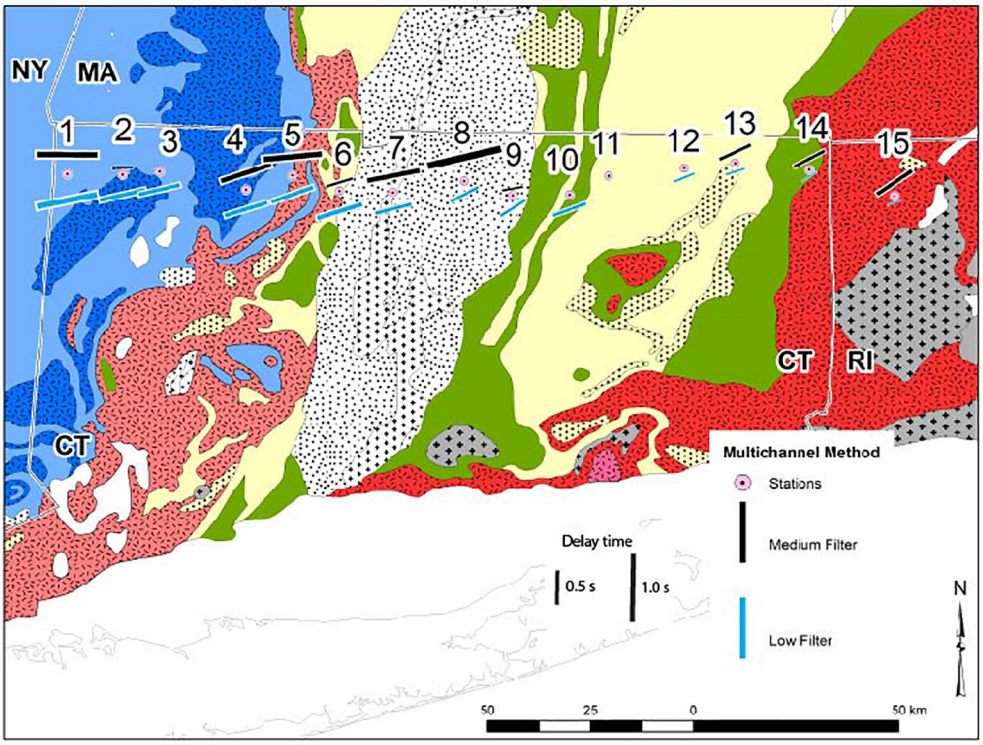

Figure 9. Map of single-station average shear wave splitting parameters, derived from the multichannel method sin(2θ) curves shown in Figure 7, plotted on top of bedrock geologic units (symbols are as in Figure 1, and map plotting conventions are as in Figure 8). We show measurements made using the medium-frequency filter (black bars; offset slightly to the north of the stations to show detail) and the low-frequency filter (blue bars; offset slightly to the south of the stations). (The high-frequency filter yielded very few splitting intensity measurements, so this frequency range is not shown.) Fast splitting orientations are indicated by the orientation of each bar; delay times are indicated by the length (and thickness) of each bar, as shown at the bottom of the figure. Delay times range from a minimum of 0.2 s (at station CS15) to a maximum of 1.1 s (at station CS08).

urements available may obscure any geographic trends. Interestingly, the general trend of decreasing delay times from west to east that is observed in the multichannel method data (Figures 7 and 9) is not evident in this subset of the TCM data (Figure 10). Histograms of ϕ observations show that fast directions are generally close to APM in the west and in the Hartford Basin, with a pronounced departure (specifically, dominantly N-S fast directions, which are observed mostly at the easternmost station of the array) for the eastern group of stations.

Single-station average splitting parameters derived from the multichannel method (Figure 9) exhibit notably less variability, and few obvious correlations with geologic structure are observed. The geographic trend of higher delay times in the west and lower delay times in the east (particularly at low frequencies) is clear on Figure 9, as is the lack of correlation between observed fast directions and geologic structures, and the presence of a slight counterclockwise rotation in fast directions towards the eastern end of the array. Station CS15 shows a substantial departure from the more nearly E-W fast directions observed elsewhere in the array, but the observed fast directions (at both medium and low frequencies) are NE-SW, rather than N-S as observed with the TCM method for this station (Figure 8).

4. Discussion

4.1. Complex and Laterally Variable SK(K)S Splitting Behavior Across Connecticut

Our study has identified average fast splitting directions of roughly 75° (or, equivalently, 255°) across the SEISConn array (with some localized exceptions, discussed further below). Estimates of the APM

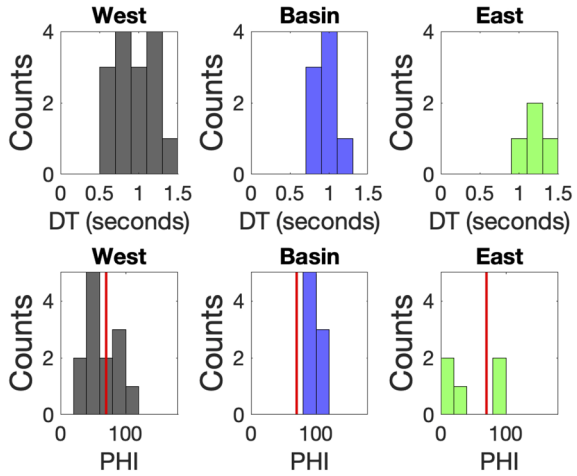

Figure 10. Histograms of measured delay times (top row) and fast splitting directions (bottom row), derived from the set of individual transverse component minimization measurements at medium frequency. Stations are divided geographically into west (CS01-CS06), basin (that is, stations located in the Mesozoic Hartford Basin in the central portion of the array; CS07-CS09), and east (CS10-CS15) groups; see Figure 2. Red lines on the bottom panels indicate the direction of local absolute plate motion (APM) of the North American plate in a hotspot reference frame, from the HS3-NUVEL1A model (Gripp & Gordon, 2002).

direction vary from ~279° to 290° in a no-net-rotation (NNR) reference frame, depending on the plate motion model (e.g., Altamimi et al., 2016; Argus et al., 2011; Kreemer et al., 2014), to ~250° in a Pacific hotspot reference frame (Gripp & Gordon, 2002). A previous comparison between SKS splitting and APM direction in northeastern North America showed that average fast directions tend to correspond better to APM estimates in a hotspot reference frame rather than an NNR reference frame (Long et al., 2016). Our fast direction observations are consistent with earlier findings in New England from the much sparser TA (e.g., Long et al., 2016; Yang et al., 2017), and are generally consistent with a scenario in which a major contributor to the SK(K)S splitting signal is shear is the asthenosphere due to the motion of the overlying North American Plate (at least in the western part of the array, where delay times are high). Based on a global study of anisotropy, Debayle and Ricard (2013) suggested that anisotropy due to APM-parallel shear in the asthenosphere is weak for plates moving at speeds smaller than 30 mm/yr and increases for plate rates between 30 and 50 mm/yr. Estimates for the motion of the North American plate range from ~15 to 33 mm/yr depending on the reference frame and plate motion model, with speeds at the high end of the range calculated for Pacific hotspot based reference frames (e.g., Gripp & Gordon, 2002). While our observations are consistent with (relatively weak) APM-parallel anisotropy beneath the western end of the SEISConn array, resulting in delay times of up to ~0.9 s, there are aspects of the SEISConn SK(K)S splitting dataset that suggest complexity beyond this relatively simple picture.

A clear finding of this study is that despite the relatively small aperture of the SEISConn deployment (~150 km), there is evidence for lateral variability in splitting behavior (and thus upper mantle anisotropy) across the array. The most prominent characteristic of this variability is the pronounced, nearly monotonic decrease in splitting delay times (as estimated using the multichannel method at low frequencies) from west to east across the SEISConn line (Figures 7 and 9). We also see evidence at a few stations for localized and specific contributions to splitting from lithospheric anisotropy that is related to specific tectonic boundaries. This is most prominent in the stations that are close to the eastern boundary of the Laurentian terrane (stations CS04, CS05, and CS06), which exhibit TCM measurements that are different from the generally E-W fast directions observed across Connecticut, and at station CS15 on the Avalon terrane, which clearly exhibits N-S fast splitting directions. These observations (made using the TCM method on medium- and high-frequency data) likely point to localized and relatively shallow anisotropic structures in the lithosphere which may contribute locally to the splitting signal. At low frequencies and using the multichannel method (which can obscure the contributions from multiple anisotropic layers), these contributions are less evident.

We also find that apparent splitting, as measured by the TCM method, varies with backazimuth at some SEISConn stations, supporting the notion of complex and laterally variable upper mantle anisotropy beneath southern New England. Single-station results showing backazimuthal variations suggest the presence of multiple layers of anisotropy (e.g., Levin et al., 1999; Menke & Levin, 2003; Silver & Savage, 1994). Unfortunately, limited data due to the short deployment times of SEISConn stations and imperfect backazimuthal distribution of events precludes a comprehensive forward modeling approach in which multiple layers of anisotropy are specifically considered. However, the complexity in the single-station stereoplots in Figure 6 supports the argument for multiple layers. Because present-day deformation from APM alone cannot explain either the backazimuthal variations in apparent splitting (Figure 6) or the (relatively modest) lateral variations in splitting behavior across the array, we propose that there are likely both asthenospheric and lithospheric contributions to splitting beneath northern Connecticut.

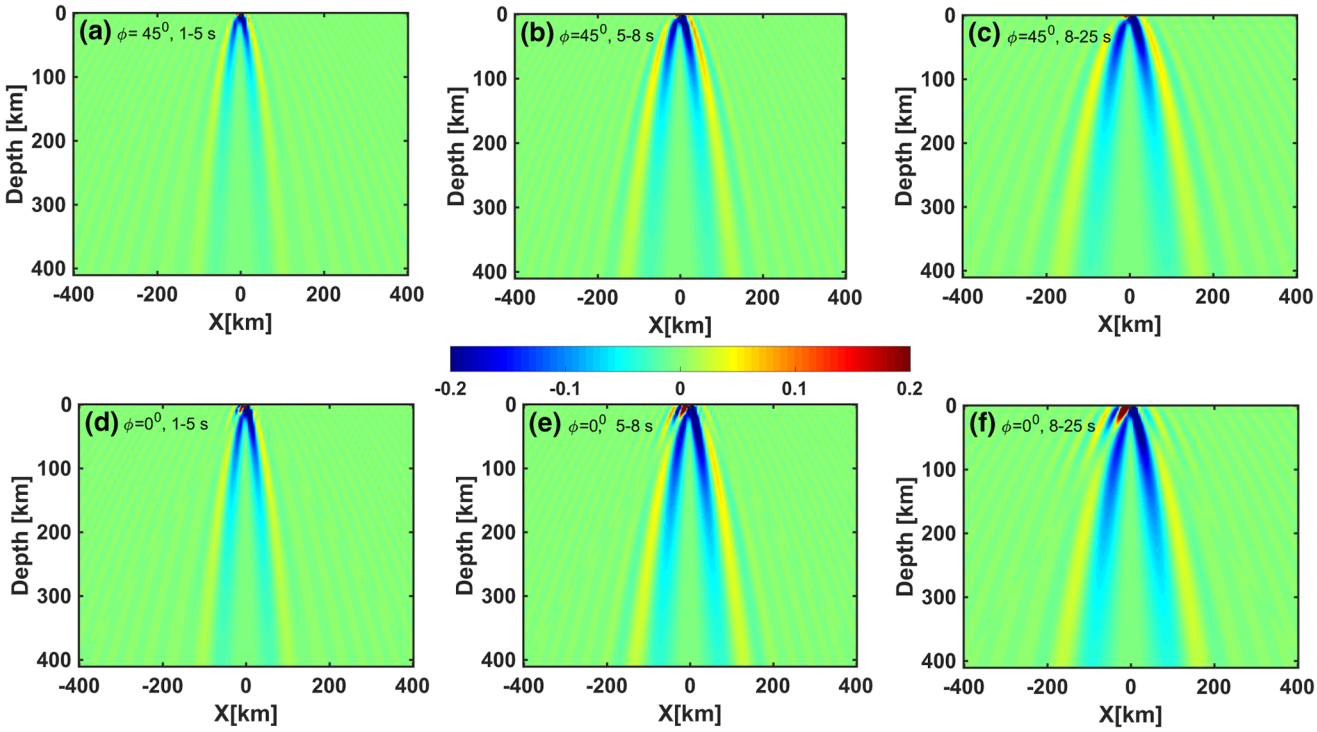

Figure 11. Examples of sensitivity kernels for SKS splitting at the frequency ranges used in this study, calculated using the method of Mondal and Long (2019). Top row shows 2-D slices through sensitivity kernels for the anisotropy strength parameter (Mondal & Long, 2019) calculated for a homogenous background model with a horizontal axis of symmetry and a fast axis at 45°, for an SKS arrival with a backazimuth of 150°. Kernels are shown for period ranges of 1–5 s (left), 5–8 s (center), and 8–25 s (right), corresponding to the high-, medium-, and low-frequency filters used in this study. Colors show sensitivity values, as shown by the colorbar, in units of 10^{-14} s/m^3. Bottom row shows sensitivity kernels calculated for a homogeneous background model with a horizontal axis of symmetry and a fast axis at 0°, again for an SKS arrival with a backazimuth of 150°, for the same set of period ranges. Note that in each case, the zone of sensitivity depends on the frequency content of the waves, with sensitivity concentrated at shallower depths for higher-frequency measurements.

4.2. Frequency Dependence of SK(K)S Splitting Parameters

A notable aspect of our SEISConn shear wave splitting dataset is that the splitting behavior (as measured with the TCM method) depends to some extent on frequency, with a much higher proportion of null measurements at low frequencies, and more lateral variability in apparent fast directions at high frequencies (Figures 6 and 8). We also see some frequency-dependent splitting behavior in the multichannel method measurements (Figures 7 and 9), manifested mainly as a difference in delay times at low versus medium frequency. Interestingly at several stations (CS08, CS13, CS14, and CS15), we document larger splitting delay times (as measured with the multichannel method) at medium frequencies than in the low-frequency band. To some extent, this dependence on frequency (specifically the high proportion of nulls at low frequencies when compared with high frequencies, as obtained with TCM) likely reflects the generally small delay times beneath Connecticut, and limitations of the TCM method, which is a more useful tool when applied to higher rather than lower frequency data when delay times are small, as discussed in Section 2.2. Beyond this methodological limitation, there are physical reasons why shear wave splitting observations may depend on frequency. Figure 11 shows examples of finite-frequency sensitivity kernels for splitting intensity observations for different frequency bands, computed using the formulation of Mondal and Long (2019). The details of the kernels depend heavily on the background model used in the kernel computation (e.g., Long et al., 2008), so they cannot be taken as a straightforward indicator of how anisotropic structure beneath the SEISConn array will be sampled. However, they illustrate the general principle that the volume of the Earth that is sampled by (in this case) SKS waves will depend on the frequency content of the waves used. The kernels shown in Figure 11, which were computed for a simple, homogeneous background model, demonstrate that high-frequency data may sample shallow structure more efficiently.

Other studies have also documented frequency-dependent shear wave splitting in a variety of tectonic settings (e.g., Eakin & Long, 2013; Long, 2010; Marson-Pidgeon & Savage, 1997), and have suggested that this frequency dependence reflects the different sampling (at different frequencies/wavelengths) of anisotropic structure with multiple layers, lateral variability, or both. Given the evidence for such variability beneath the SEISConn array (discussed in Section 4.1), we suggest the following scenario. At low frequencies, we sample the deeper (asthenospheric) parts of the system more efficiently, and thus our results using the low-frequency multichannel method, which exhibit generally nearly E-W fast directions and gradual lateral variations in delay times, generally reflect the asthenospheric contribution to the splitting signal. At higher frequencies, we preferentially sample the shallower (mantle lithospheric, with perhaps a small contribution from the crust as well) portions of the system, and thus the lithospheric contributions are more prominent in the high-frequency measurements.

4.3. SK(K)S Splitting at Terrane Boundaries and Regional Anisotropic Domains

As discussed in Section 4.1, we have documented apparent splitting measurements using the TCM method at two groups of stations (CS04-CS06 and CS14-CS15) that are different from the generally nearly E-W fast directions that are observed with the TCM method at other SEISConn stations, and with the multichannel method across the entire array. The first group of stations (CS04-CS06) exhibits a complex mix of apparent fast directions (Figure 8); a subgroup of these exhibits orientations that are nearly NE-SW, parallel to the local strike of the nearby terrane boundary between Laurentia (to the west) and the Moretown terrane (to the east). The second group (CS14-CS15) is located at the eastern end of the array, close to the boundary between the Avalon terrane (to the east) and the Putnam-Nashoba belt (to the west). Station CS15 exhibits uniformly N-S fast splitting directions at both medium and high frequency, while station CS14 exhibits E-W fast directions at medium frequency and NNE-SSW fast directions at high frequency. The local strike of the terrane boundary (the Lake Char-Honey Hill fault) is N-S, parallel to the fast splitting directions at CS15. We speculate that these deviations from the overall average splitting pattern beneath northern Connecticut represent localized contributions to splitting from lithospheric deformation (perhaps including both the crust and the mantle lithosphere) associated with subduction, collision, and terrane accretion during Appalachian orogenesis. Orogen-parallel fast splitting directions have been documented elsewhere in the Appalachians (e.g., Barruol et al., 1997; Long et al., 2016; Wagner et al., 2012; White-Gaynor & Nyblade, 2017) and have been attributed to vertically coherent deformation of the mantle lithosphere during compression and shortening (Silver, 1996).

Li et al. (2019) examined long-running seismic stations in the northeastern U.S. and found evidence for distinct, localized anisotropic domains based on coherent splitting behavior observed at sets of stations within particular geographic regions (Figure 12). Specifically, they identified a region of weak splitting, with stations dominated by a high percentage of null (non-split) SKS arrivals, that included the NAA region in New Hampshire and Vermont and extended to the south and east to include eastern Massachusets, Rhode Island, and the easternmost part of Connecticut. They characterized the western part of Connecticut as being part of a domain that extends west through southern New York, northern New Jersey, and eastern Pennsylvania. This domain has slightly stronger splitting than the NAA domain (but still weaker than the regional average), with a bimodal population of individual fast splitting direction estimates. While the long-running stations used by Li et al. (2019) allowed for a much more detailed characterization of splitting behavior at each station, the comparatively short-lived SEISConn array offers the advantage of a much larger number of stations. The Li et al. (2019) study included data from just one station in northern Connecticut (UCCT, located just to the south of SEISConn), while our dataset, with 15 stations, allows us to probe the anisotropic boundary proposed by Li et al. (2019) in greater detail and at higher resolution.

Figure 12 shows our single-station average splitting measurements (as derived from the multichannel method using the low-frequency filter) plotted on top of the anisotropic domains proposed by Li et al. (2019). Single-station average measurements obtained using the splitting intensity method by Li et al. (2019) are also shown for comparison. We note that measurements obtained using other methods (e.g., Long et al., 2016; Yang et al., 2017) are not shown on this map; they are not directly

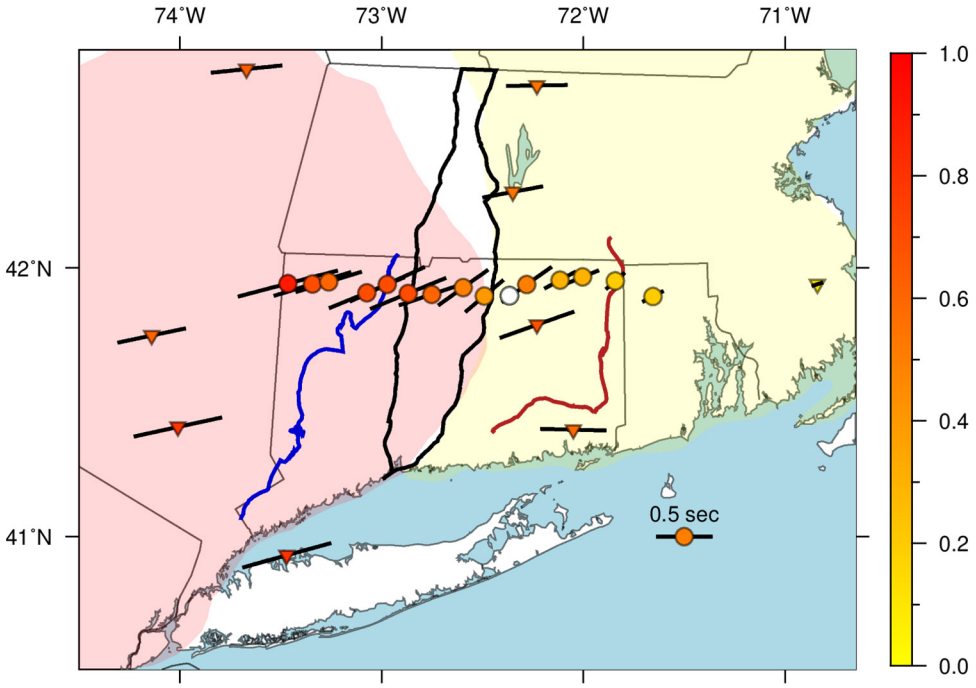

Figure 12. Map of regional anisotropic domains (yellow and red shading) delineated by Li et al. (2019), along with our measurements of single-station (circles) average fast directions and delay times, as derived from the multichannel method using the low-frequency filter. Orientation of black bars indicate the fast splitting direction, while the delay time is indicated both by the length of the bar (as indicated by the scale bar) and by the color of the station symbol (as indicated by color bar at right). One station (CS10, white circle; see also Figure 9) did not have sufficient splitting intensity measurements to reliably retrieve splitting parameters. Thick lines indicate major tectonic boundaries, as in Figure 2. Previous measurements of Li et al. (2019), which were used to delineate the anisotropic domains shown with yellow and red shading, are also shown (stations indicated with triangles). We show the single-station splitting parameters from Li et al. (2019) derived from splitting intensity measurements, so they are directly comparable to the measurements shown at SEISConn stations. SEISConn, Seismic Experiment for Imaging Structure Beneath Connecticut.

comparable, and observed delay times tend to be substantially higher. Our measurements are consistent with the characteristics of these previously defined anisotropic domains, with very weak splitting in the eastern part of the SEISConn array and somewhat stronger splitting in the western portion. Our observation of backazimuthal variations at SEISConn stations is also generally consistent with the findings of Li et al. (2019), and compatible with their suggestion that both the asthenosphere and lithosphere likely contribute to shear wave splitting observations beneath the northeastern U.S. With the dense station spacing afforded by SEISConn, we can characterize the boundary between the two anisotropic domains in Connecticut as relatively gradual, rather than sharp (Figure 11), and the transition in splitting behavior from west to east may reflect changes in both the lithosphere and the asthenosphere.

4.4. Possible Models for Upper Mantle Anisotropy Beneath Southern New England

Given the insights into the likely vertical and lateral distribution of seismic anisotropy beneath southern New England we have gained from the SEISConn data set, what is the most likely scenario for controls on asthenospheric and lithospheric anisotropy? Key observations include the mainly APM-parallel fast splitting directions (particularly as expressed in the multichannel method), the backazimuthally varying and frequency-dependent nature of the splitting observations (particularly as expressed in the TCM method), the clear trend of decreasing splitting delay times from west to east (particularly at low frequencies), and the observations of a few stations that exhibit fast splitting directions that are parallel to local terrane bounda-

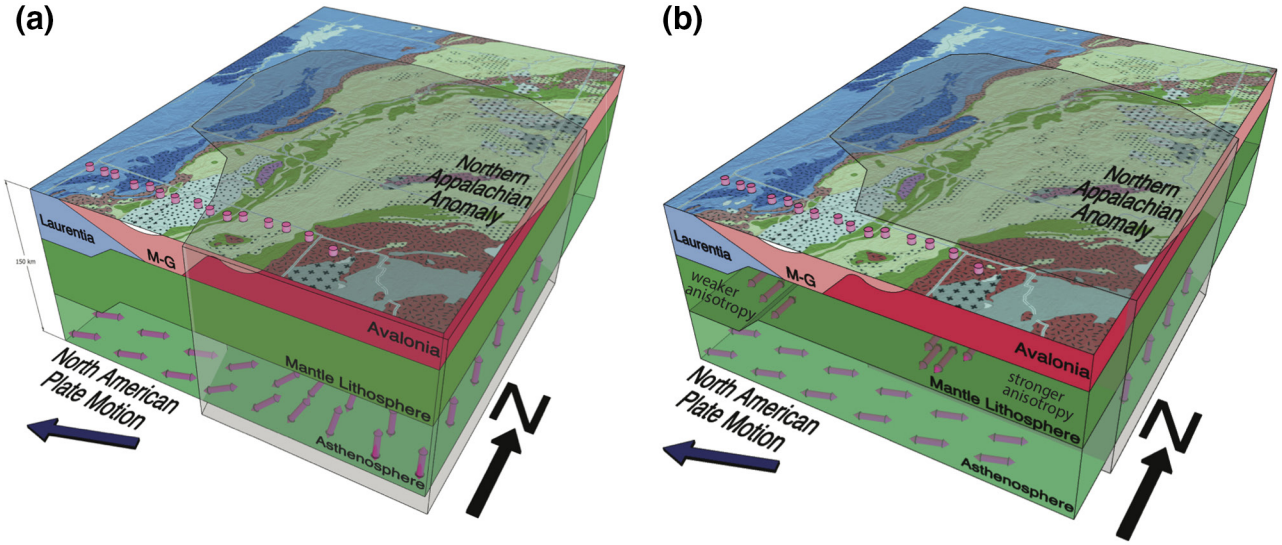

Figure 13. Block diagrams showing possible endmember models that can explain the SEISConn splitting observations, with bedrock geology shown at the surface and a schematic cartoon of anisotropic structure in the mantle lithosphere (dark green) and asthenosphere (light green). (a) A scenario that invokes a transition in asthenospheric mantle flow (pink arrows), from plate-motion-parallel shearing in the west to vertical flow in the east, due to upper mantle upwelling associated with the Northern Appalachian Anomaly (NAA) (shaded region). Splitting is mostly controlled by anisotropy in the asthenosphere, with minimal contributions from the lithosphere. (b) A scenario in which the lateral variations in anisotropy are controlled mainly by anisotropy in the lithosphere. The generally E-W fast directions in the asthenosphere (due to absolute plate motion [APM]) are canceled out, to varying degrees, by dominantly north-south oriented anisotropy in the mantle lithosphere. In the west, the lithospheric contribution is relatively weak and the APM-parallel anisotropy in the asthenosphere dominates the signal; in the east, the lithospheric contribution is relatively strong and there is destructive interference between the two anisotropic layers, resulting in small splitting delay times. Contributions to splitting from lithospheric anisotropy is locally strong near major terrane boundaries (pink arrows in the lithospheric mantle). In this scenario, upwelling in the asthenospheric upper mantle associated with the NAA (shaded region) is limited to the region north of the SEISConn array. SEISConn, Seismic Experiment for Imaging Structure Beneath Connecticut.

ries (particularly at high frequencies). Given this set of observations, it is highly likely that there are some contributions from both the asthenosphere and the lithosphere.

We consider two endmember scenarios, shown in Figure 13, which are capable of explaining the gradual decay of splitting delay times from west to east across the array (Figure 12). The first invokes a transition in flow regime in the asthenospheric mantle as the primary reason for the change in the strength of shear wave splitting. In this scenario, the asthenosphere is dominated by APM-parallel shearing beneath western Connecticut, and there is a transition to vertical upwelling flow beneath eastern Connecticut. The zone of upper mantle upwelling associated with the NAA proposed by Levin et al. (2018) extends as far south as the SEISConn array location (roughly 42° latitude) in the eastern portion of Connecticut. This view is consistent with the proposal by Li et al. (2019) that the anisotropic domain associated with the NAA (characterized by weak SKS splitting) centered in Vermont and New Hampshire extends to southeastern Massachusetts, Rhode Island, and eastern Connecticut. In this scenario, anisotropy in the mantle lithosphere throughout Connecticut is probably generally weak, with the exception of regions of locally strong anisotropy near major terrane boundaries (the eastern edge of Laurentia and the western edge of the Avalon terrane). This model invokes vertical mantle flow associated with edge-driven convection as an explanation for weak splitting at the eastern end of SEISConn, as envisioned by Levin et al. (2018) and Menke et al. (2016) for the NAA, and based on numerical models of flow associated with edge-driven convection cells (King & Anderson, 1998).

An alternative model that might explain the lateral variability in delay times invokes lithospheric anisotropy, rather than present-day mantle flow, as a primary explanation (Figure 13). In this view, the upper mantle anisotropy signature beneath western Connecticut is dominated by APM-parallel shearing in the asthenosphere, which produces ~0.9 s of SK(K)S splitting with a fast direction that is parallel to APM, and the lithospheric contribution to anisotropy is negligible (perhaps with a local exception close to the boundary between the Laurentian and Moretown terranes). Moving to the east, the strength of

anisotropy in the lithosphere steadily increases, and its geometry is such that there is destructive interference between two layers of anisotropy: one in the asthenosphere with a generally E-W fast direction, and one in the lithosphere with a generally N-S fast direction. In this scenario, the lithospheric fabric leads to fast splitting directions (due to the lithosphere) that are oriented N-S; a reasonable explanation for such a fabric would be vertically coherent, compressive deformation (Silver, 1996) of the lithosphere during Appalachian orogenesis, as has been proposed elsewhere in the Appalachians (e.g., Barruol et al., 1997; Long et al., 2016; White-Gaynor & Nyblade, 2017). In order for this model to explain the decrease in delay times from west to east, the strength of lithospheric anisotropy would need to steadily increase from west to east, although it may be locally stronger near terrane boundaries (which would explain the observations at medium and high frequencies at stations CS04-CS06 and CS14-CS15).

These are endmember scenarios, and it is possible (perhaps likely) that the actual Earth structure incorporates elements of both ideas. On balance, we find the idea of a transition to upwelling flow in the upper mantle at the eastern end of the SEISConn array (Figure 13a) to be compelling, since Li et al. (2019) has persuasively demonstrated that the region of weak splitting in eastern Connecticut is connected geographically with the region of weak splitting above the NAA first documented by Levin et al. (2018). While a scenario in which pervasive N-S oriented anisotropy in the mantle lithosphere exhibits lateral variability in its strength, with weak lithospheric anisotropy in the west and strong lithospheric anisotropy in the east (Figure 13b), is also possible, we do not have a ready explanation for why such a variation in lithospheric anisotropy strength would be present. Even if our preferred scenario of a transition in upper mantle flow regime (Figure 13a) does provide the first-order explanation for the variation in delay times across the SEISConn array, it is clear that there must also be some lithospheric contribution to splitting as well. If the mantle flow transition scenario is correct, then the lithospheric anisotropy is likely relatively weak throughout much of the study area, with local exceptions near the terrane boundaries. Our finding that strong anisotropy in the mantle lithosphere (perhaps with a contribution from the crust as well) near terrane boundaries is required to explain our data suggests that the lithosphere was strongly deformed via the processes of subduction and terrane accretion during Appalachian orogenesis. This deformation, however, may have been relatively limited in spatial extent (perhaps only 10 s of km).

Distinguishing confidently between the models shown in Figure 13, and quantifying the relative contributions of lithospheric versus asthenospheric anisotropy across the SEISConn array, will require complementary constraints from seismic observations that do not share the limitations on depth resolution of SK(K)S splitting analysis. Fortunately, there are a number of tools that can constrain the depth distribution of anisotropy that are available for future analyses, and which will be applied to data from SEISConn and other regional networks in the future. These include anisotropy-aware receiver function analysis (e.g., Long et al., 2017; Yuan & Levin, 2014), which can delineate layered anisotropy in the crust and lithospheric mantle, surface wave-based tomography models that include azimuthal anisotropy (e.g., Wagner et al., 2018), analysis of Love-to-Rayleigh surface wave scattering (e.g., Servali et al., 2020), SKS splitting intensity tomography (e.g., Mondal & Long, 2020), and anisotropic Pn tomography (e.g., Buehler & Shearer, 2017).

5. Conclusions

We have investigated SK(K)S splitting across the dense SEISConn array in northern Connecticut and Rhode Island. We found evidence for relatively weak splitting with generally nearly E-W fast directions, almost parallel to the absolute motion of the North American plate. At low frequencies, we documented a pronounced and steady decrease of delay times from west to east beneath the array. At medium and high frequencies, the measurements are more scattered, and there is evidence for multiple layers of anisotropy and for locally strong contributions to splitting from the lithosphere near major terrane boundaries. We favor a scenario in which there is a lateral transition in the asthenospheric mantle from plate-motion-parallel shearing beneath western Connecticut to vertical upwelling flow beneath eastern Connecticut and Rhode Island, associated with the NAA upper mantle seismic anomaly that is centered to the north. In addition to the contributions to splitting from the asthenospheric upper mantle, there are modest contributions from the lithosphere (the mantle and perhaps the crust) as well. Throughout much of the study area, the strength of lithospheric ani-

sotropy seems to be relatively weak, but there are locally strong regions near major terrane boundaries (the eastern edge of the Laurentian terrane and the western edge of the Avalon terrane). This locally prominent anisotropy reflects strong, but spatially limited, deformation of the crust and mantle lithosphere associated with terrane accretion during Appalachian orogenesis. Future application of seismic analysis techniques that can better delineate the depth distribution of anisotropy beneath the southern New England Appalachians will help to constrain models for present-day mantle flow and past lithospheric deformation, and to quantify the relative contributions of the lithosphere versus the asthenosphere to SK(K)S splitting observations.

Data Availability Statement

Waveform data from the SEISConn experiment (network code XP; doi:10.7914/SN/XP_2015) are archived at the IRIS DMC (https://ds.iris.edu/ds/nodes/dmc) and will be publicly available from August 2021.

Acknowledgments
We thank personnel at the IRIS DMC for facilitating the archiving of SEISConn data. The facilities of the IRIS Consortium were supported by the U.S. National Science Foundation Seismological Facilities for the Advancement of Geoscience (SAGE) Award, Cooperative Support Agreement EAR-1851048. The SEISConn project has been funded by Yale University and by NSF via grants EAR-1150722 and EAR-1800923 to M. D. Long. This research was initiated during a summer research internship that was funded by Williams College. We are profoundly grateful to all landowners who graciously hosted SEISConn stations. We thank all field volunteers who contributed to the SEISConn deployment, particularly participants in the Field Experiences for Science Teachers (FEST) program (Long, 2017). We are grateful to all of our scientific collaborators on various aspects of the SEISConn data analysis and interpretation, and other projects in New England, for useful discussions. We thank Vadim Levin in particular for useful discussions on SKS splitting in New England and for assistance with plotting scripts, and we thank Puskar Mondal for assistance with drafting Figure 11. We are grateful to the Associate Editor and to two anonymous reviewers for thoughtful and constructive comments that helped us to improve the paper.

References

Altamimi, Z., Rebischung, P., Métivier, L., & Collilleux, X. (2016). ITRF2014: A new release of the International Terrestrial Reference Frame modeling nonlinear station motions. *Journal of Geophysical Research*, *121*, 6109–6131. https://doi.org/10.1002/2016JB013098

Amidon, W. H., Roden-Tice, M., Anderson, A. J., McKeon, R. E., & Shuster, D. L. (2016). Late Cretaceous unroofing of the White Mountains, New Hampshire, USA: An episode of passive margin rejuvenation?. *Geology*, *44*(6), 415–418. https://doi.org/10.1130/G37429.1

Aragon, J. C., Long, M. D., & Benoit, M. H. (2017). Lateral variations in SKS splitting across the MAGIC array, Central Appalachians. *Geochemistry, Geophysics, Geosystems*, *18*, 4136–4155. https://doi.org/10.1002/2017GC007169

Argus, D. F., Gordon, R. G., & DeMets, C. (2011). Geologically current motion of 56 plates relative to the no-net-rotation reference frame. *Geochemistry, Geophysics, Geosystems*, *12*, Q11001. https://doi.org/10.1029/2011GC003751

Asplet, J., Wookey, J. M., & Kendall, J. M. (2020). A potential post-perovskite province in D" beneath the Eastern Pacific: Evidence from new analysis of discrepant SKS-SKKS shear-wave splitting. *Geophysical Journal International*, *221*, 2075–2090. https://doi.org/10.1093/gji/ggaa114

Barruol, G., & Mainprice, D. (1993). A quantitative evaluation of the contribution of crustal rocks to the shear-wave splitting of teleseismic SKS waves. *Physics of the Earth and Planetary Interiors*, *78*, 281–300. https://doi.org/10.1016/0031-9201(93)90161-2

Barruol, G., Silver, P. G., & Vauchez, A. (1997). Seismic anisotropy in the eastern United States: Deep structure of a complex continental plate. *Journal of Geophysical Research*, *102*, 8329–8348. https://doi.org/10.1029/96JB038000

Bradley, D. C., Tucker, R. D., Lux, D. R., Harris, A. G., & McGregor, D. C. (2000). Migration of the Acadian orogen and foreland basin across the northern Appalachians of Maine and adjacent areas. U.S. Geological Survey Professional Paper no. 1624. https://doi.org/10.3133/pp1624

Buehler, J. S., & Shearer, P. M. (2017). Uppermost mantle seismic velocity structure beneath USArray. *Journal of Geophysical Research: Solid Earth*, *122*(1), 436–448. https://doi.org/10.1002/2016JB013265

Chen, X., Li, Y., & Levin, V. (2018). Shear wave splitting beneath eastern North American continent: Evidence for a multi-layered and laterally variable anisotropic structure. *Geochemistry, Geophysics, Geosystems*, *19*, 2857–2871. https://doi.org/10.1029/2018GC007646

Chevrot, S. (2000). Multichannel analysis of shear wave splitting. *Journal of Geophysical Research*, *105*, 21579–21590. https://doi.org/10.1029/200JB900199

Chevrot, S. (2006). Finite-frequency vectorial tomography: A new method for high-resolution imaging of upper mantle anisotropy. *Geophysical Journal International*, *165*, 641–657. https://doi.org/10.1111/j.1365-246X.2006.02982.x

Debayle, E., & Ricard, Y. (2013). Seismic observations of large-scale deformation at the bottom of fast-moving plates. *Earth and Planetary Science Letters*, *376*, 165–177. https://doi.org/10.1016/j.epsl.2013.06.025

Deng, J., Long, M. D., Creasy, N., Wagner, L., Beck, S., Zandt, G., et al. (2017). Lowermost mantle anisotropy near the eastern edge of the Pacific LLSVP: Constraints from SKS-SKKS splitting intensity measurements. *Geophysical Journal International*, *210*, 774–786 https://doi.org/10.1093/gji/ggx190

Diaz, J., Gallart, J., Villasenor, A., Mancilla, F., Pazos, A., Cordoba, D., et al. (2010). Mantle dynamics beneath the Gibraltar Arc (western Mediterranean) from shear-wave splitting measurements on a dense seismic array. *Geophysical Research Letters*, *37*, L18304. https://doi.org/10.1029/2010GL044201

Doll, C. G., Billings, M. P., Cady, W. M., & Thompson, J. B. (Eds.). (1961). *Centennial geologic map of Vermont*. Vermont Geological Survey, Vermont Development Department.

Dong, M. T., & Menke, W. H. (2017). Seismic high attenuation region observed beneath southern New England from teleseismic body wave spectra: Evidence for high asthenospheric temperature without melt. *Geophysical Research Letters*, *44*, 10,958–10,969. https://doi.org/10.1002/2017GL074953

Eakin, C. M., & Long, M. D. (2013). Complex anisotropy beneath the Peruvian flat slab from frequency-dependent, multiple-phase shear wave splitting analysis. *Journal of Geophysical Research*, *118*, 4794–4813. https://doi.org/10.1002/jgrb.50349

Favier, N., & Chevrot (2003). Sensitivity kernels for shear wave splitting in transverse isotropic media. *Geophysical Journal International*, *156*(3), 467–482. https://doi.org/10.1046/j.1365-246X.2003.01894.x

Gao, H., Yang, X., Long, M. D., & Aragon, J. C. (2020). Seismic evidence for crustal modification beneath the Hartford Rift Basin in the Northeastern United States. *Geophysical Research Letters*, *47*, e2020GL089316. https://doi.org/10.1029/2020GL089316

Gilligan, A., Bastow, I. D., Watson, E., Darbyshire, F. A., Levin, V., Menke, W., et al. (2016). Lithospheric deformation in the Canadian Appalachians: Evidence from shear wave splitting. *Geophysical Journal International*, *206*, 1273–1280. https://doi.org/10.1093/gji/ggw207

Golos, E. M., Fang, H., Yao, H., Zhang, H., Burdick, S., & Vernon, F. (2018). Shear wave tomography beneath the United States using a joint inversion of surface and body waves. *Journal of Geophysical Research: Solid Earth*, *123*(6), 5169–5189. https://doi.org/10.1029/2017JB014894

Gonzalez, J. P., Baldwin, S. L., Thomas, J. B., Nachlas, W. O., & Fitzgerald, P. G. (2020). Evidence for ultrahigh-pressure metamorphism discovered in the Appalachian orogen. *Geology*, *48*, 947–951. https://doi.org/10.1130/G47507.1

Gripp, A. E., & Gordon, R. G. (2002). Young tracks of hotspots and current plate velocities. *Geophysical Journal International*, *150*(2), 321–361. https://doi.org/10.1046/j.1365-246X.2002.01627.x

Hatcher, R. D. (2010). The Appalachian orogen: A brief summary. In R. P. Tollo, et al. (Eds.), *From Rodinia to Pangea: The Lithotectonic Record of the Appalachian Region* (Vol. 206, pp. 1–19). Geological Society of America Memoir. https://doi.org/10.1130/2010.1206(01)

Hibbard, J. P., Van Staal, C. R., Rankin, D. W., & Williams, H. (2006). Lithotectonic map of the Appalachian orogen, Canada–United States of America. *Geological Survey of Canada, Map A*, *2096*, 2. https://doi.org/10.4095/221912

Karabinos, P., & Aleinikoff, J. N. (1990). Evidence for a major middle Proterozoic, post-Grenvillian igneous event in western New England. *American Journal of Science*, *290*(8), 959–974. doi: https://doi.org/10.2475/ajs.290.8.959

Karabinos, P., Macdonald, F. A., & Crowley, J. L. (2017). Bridging the gap between the foreland and hinterland I: Geochronology and plate tectonic geometry of Ordovician magmatism and terrane accretion on the Laurentian margin of New England. *American Journal of Science*, *317*(5), 515–554. https://doi.org/10.2475/05.2017.01

Karabinos, P., Morris, D., Hamilton, M., & Rayner, N. (2008). Age, origin, and tectonic significance of Mesoproterozoic and Silurian felsic sills in the Berkshire massif, Massachusetts. *American Journal of Science*, *308*(6), 787–812. https://doi.org/10.2475/06.2008.03

Karato, S., Jung, H., Katayama, I., & Skemer, P. (2008). Geodynamic significance of seismic anisotropy of the upper mantle: New insights from laboratory studies. *Annual Review of Earth and Planetary Sciences*, *36*, 59–95. https://doi.org/10.1146/annurev.earth.36.031207

King, S. D., & Anderson, D. L. (1998). Edge-driven convection. *Earth and Planetary Science Letters*, *160*, 289–296. https://doi.org/10.1026/S0012-821X(98)00089-2

Kinney, S., Maclennan, S. A., Setera, J., Schoene, B., VanTongeren, J., Strauss, J. V., et al. (2020). Long-lived and localized post-orogenic magmatism on the eastern North American margin: Insights from zircon U-PB geochronology. *Geological Society of America Abstracts with Programs*, *52*(2), 14-9. https://doi.org/10.1130/abs/2020SE-345449

Kreemer, C., Blewitt, G., & Klein, E. C. (2014). A geodetic plate motion and Global Strain Rate Model. *Geochemistry, Geophysics, Geosystems*, *15*, 3849–3889. https://10.1002/2014GC005407

Laird, J., Lanphere, M. A., & Albee, A. L. (1984). Distribution of Ordovician and Devonian metamorphism in mafic and pelitic schists from northern Vermont. *American Journal of Science*, *284*(4–5), 376–413. https://doi.org/10.2475/ajs.284.4-5.376

Lei, W., & Wen, L. (2020). Widespread small-scale anisotropic structure in the lowermost mantle beneath the North American continent and Northeastern Pacific. *Seismological Research Letters*, *91*, 2779–2790. https://doi.org/10.1785/0220200055

Levin, V., Long, M. D., Skryzalin, P., Li, Y., & López, I. (2018). Seismic evidence for a recently formed mantle upwelling beneath New England. *Geology*, *46*, 87–90. https://doi.org/10.1130/G39641.1

Levin, V., Menke, W., & Park, J. (1999). Shear wave splitting in the Appalachians and the Urals: A case for multilayered anisotropy. *Journal of Geophysical Research*, *104*, 17975–17993. https://doi.org/10.1029/1999JB900168

Li, Y., Levin, V., Elkington, S., & Hlavaty, J. (2019). Localized anisotropic domains beneath eastern North America. *Geochemistry, Geophysics, Geosystems*, *20*, 5499–5521. https://doi.org/10.1029/2019GC008518

Long, M. D. (2010). Frequency-dependent shear wave splitting and heterogeneous anisotropic structure beneath the Gulf of California region. *Physics of the Earth and Planetary Interiors*, *182*, 59–72. https://doi.org/10.1016/j.pepi.2010.06.005

Long, M. D. (2017). The Field Experiences for Science Teachers (FEST) project: Involving high school science teachers in field seismology. *Seismological Research Letters*, *88*, 421–429. https://doi.org/10.1785/0220160162

Long, M. D., & Aragon, J. A. (2020). Probing the structure of the crust and mantle lithosphere beneath the Southern New England Appalachians via the SEISConn deployment. *Seismological Research Letters*, *91*, 2976–2986. https://doi.org/10.1785/02202000163

Long, M. D., Benoit, M. H., Chapman, M. C., & King, S. D. (2010). Upper mantle anisotropy and transition zone thickness beneath southeastern North America and implications for mantle dynamics. *Geochemistry, Geophysics, Geosystems*, *11*, Q10012. https://doi.org/10.1029/2010GC003247

Long, M. D., De Hoop, M. V., & Van Der Hilst, R. D. (2008). Wave-equation shear wave splitting tomography. *Geophysical Journal International*, *172*(1), 311–330. https://doi.org/10.1111/j.1365-246X.2007.03632.x

Long, M. D., Ford, H. A., Abrahams, L., & Wirth, E. A. (2017). The seismic signature of lithospheric deformation due to Grenville and Appalachian orogenesis beneath eastern North America. *Lithosphere*, *9*, 987–1001. https://doi.org/10.1130/L660.1

Long, M. D., Jackson, K. G., & McNamara, J. F. (2016). SKS splitting beneath Transportable Array stations in eastern North America and the signature of past lithospheric deformation. *Geochemistry, Geophysics, Geosystems*, *17*, 2–15. https://doi.org/10.1029/2015GC006088

Long, M. D., & Silver, P. G. (2009). Shear wave splitting and mantle anisotropy: Measurements, interpretations, and new directions. *Surveys in Geophysics*, *30*(4), 407–461. https://doi.org/10.1007/S10712-009-9075-1

Lutz, K. A., Long, M. D., Creasy, N., & Deng, J. (2020). Seismic anisotropy in the lowermost mantle beneath North America from SKS-SKKS splitting intensity discrepancies. *Physics of the Earth and Planetary Interiors*, *305*, 106504. https://doi.org/10.1016/j.pepi.2020.106504

Macdonald, F. A., Karabinos, P. M., Crowley, J. L., Hodgin, E. B., Crockford, P. W., & Delano, J. W. (2017). Bridging the gap between the foreland and hinterland II: Geochronology and tectonic setting of Ordovician magmatism and basin formation on the Laurentian margin of New England and Newfoundland. *American Journal of Science*, *317*(5), 555–596. https://doi.org/10.2475/05.2017.02

Macdonald, F. A., Ryan-Davis, J., Coish, R. A., Crowley, J. L., & Karabinos, P. (2014). A newly identified Gondwanan terrane in the northern Appalachian Mountains: Implications for the Taconic orogeny and closure of the Iapetus Ocean. *Geology*, *42*(6), 539–542. https://doi.org/10.1130/G35659.1

Marson-Pidgeon, K., & Savage, M. K. (1997). Frequency-dependent anisotropy in Wellington, New Zealand. *Geophysical Research Letters*, *24*, 3297–3300. https://doi.org/10.1029/97GL03274

Marzoli, A., Renne, P. R., Piccirillo, E. M., Ernesto, M., Bellieni, G., & De Min, A. (1999). Extensive 200-million-year-old continental flood basalts of the Central Atlantic Magmatic Province. *Science*, *284*(5414), 616–618. https://doi.org/10.1126/science.284.5414.616

Menke, W., Lamoureux, J., Abbott, D., Hopper, E., Hutson, D., & Marrero, A. (2018). Crustal heating and lithospheric alteration and erosion associated with asthenospheric upwelling beneath southern New England (USA). *Journal of Geophysical Research: Solid Earth*, *123*(10), 8995–9008. https://doi.org/10.1029/2018JB015921

Menke, W., & Levin, V. (2003). The cross-convolution method for interpreting SKS splitting observations, with application to one and two-layer anisotropic earth models. *Geophysical Journal International*, *154*(2), 379–392. https://doi.org/10.1046/j.1365-246X.2003.01937.x

Menke, W., Skryzalin, P., Levin, V., Harper, T., Darbyshire, F., & Dong, T. (2016). The Northern Appalachian Anomaly: A modern asthenospheric upwelling. *Geophysical Research Letters*, *43*, 10,173–10,179. https://doi.org/10.1002/2016GL070918

Mondal, P., & Long, M. D. (2019). A model space search approach to finite-frequency SKS splitting intensity tomography in a reduced parameter space. *Geophysical Journal International*, *217*, 238–256. https://doi.org/10.1093/gji/ggz016

Mondal, P., & Long, M. D. (2020). Strong seismic anisotropy in the deep upper mantle beneath the Cascadia backarc: Constraints from probabilistic finite-frequency SKS splitting intensity tomography. *Earth and Planetary Science Letters*, *539*, 116172. https://doi.org/10.1016/j.epsl.2020.116172

Monteiller, V., & Chevrot, S. (2010). How to make robust splitting measurements for single-station analysis and three dimensional imaging of seismic anisotropy. *Geophysical Journal International*, *182*(1), 311–328. https://doi.org/10.1111/j.1365-246X.2010.04608.x

Olsen, P. E. (1997). Stratigraphic record of the early Mesozoic breakup of Pangea in the Laurasia-Gondwana rift system. *Annual Review of Earth and Planetary Sciences*, *25*(1), 337–401. https://doi.org/10.1146/annurev.earth.25.1.337

Pazzaglia, F. J., & Brandon, M. T. (1996). Macrogeomorphic evolution of the post-Triassic Appalachian mountains determined by deconvolution of the offshore basin sedimentary record. *Basin Research*, *8*(3), 255–278. https://doi.org/10.1046/j.1365-2117.1996.00274.x

Polet, J., & Kanamori, H. (2002). Anisotropy beneath California: Shear wave splitting measurements using a dense broadband array. *Geophysical Journal of International*, *149*, 313–327. https://doi.org/10.1046/j.1365-246X.2002.01630.x

Porter, R., Liu, Y., & Holt, W. E. (2016). Lithospheric records of orogeny within the continental US. *Geophysical Research Letters*, *43*(1), 144–153. https://doi.org/10.1002/2015GL066950

Ratcliffe, N. M., & Zartman, R. E. (1976). Stratigraphy, isotopic ages, and deformational history of basement and cover rocks of the Berkshire Massif, southwestern Massachusetts. *Geological Society of America Memoir*, *148*, 373–412. https://doi.org/10.1130/MEM148-p373

Reiss, M. C., Long, M. D., & Creasy, N. (2019). Lowermost mantle anisotropy beneath Africa from differential SKS-SKKS shear-wave splitting. *Journal of Geophysical Research: Solid Earth*, *124*, 8540–8564. https://doi.org/10.1029/2018JB017160

Reiss, M. C., & Rümpker, G. (2017). SplitRacer: MATLAB Code and GUI for semiautomated analysis and interpretation of teleseismic shear-wave splitting. *Seismological Research Letters*, *88*(2A), 392–409. https://doi.org/10.1785/0220160191

Rümpker, G., Ryberg, T., & Bock, G., & DESERT Seismology Group. (2003). Boundary-layer mantle flow under the Dead Sea transform fault € inferred from seismic anisotropy. *Nature*, *425*, 497–501. https://doi.org/10.1038/nature01982

Ryberg, T., Rümpker, G., Haberland, C., Stromeyer, D., & Weber, M. (2005). Simultaneous inversion of shear wave splitting observations from seismic arrays. *Journal of Geophysical Research: Solid Earth*, *110*, B03301. https://doi.org/10.1029/2004JB003303

Savage, B., Covellone, B. M., & Shen, Y. (2017). Wave speed structure of the eastern North American margin. *Earth and Planetary Science Letters*, *459*, 394–405. https://doi.org/10.1016/j.epsl.2016.11.028

Schmandt, B., & Lin, F. C. (2014). P and S wave tomography of the mantle beneath the United States. *Geophysical Research Letters*, *41*, 6342–6349. https://doi.org/10.1002/2014GL061231

Servali, A., Long, M. D., Park, J., Benoit, M. H., & Aragon, J. C. (2020). Love-to-Rayleigh scattering across the Eastern North American Margin. *Tectonophysics*, *776*, 228321. https://doi.org/10.1016/j.tecto.2020.228321

Sieminski, A., Paulssen, H., Trampert, J., & Tromp, J. (2008). Finite-frequency SKS splitting: Measurement and sensitivity kernels. *Bulletin of the Seismological Society of America*, *98*(4), 1797–1810. https://doi.org/10.1785/0120070297

Silver, P. G. (1996). Seismic anisotropy beneath the continents: Probing the depths of geology. *Annual Review of Earth and Planetary Sciences*, *24*(1), 385–432. https://doi.org/10.1146/annurev.earth.24.1.385

Silver, P. G., & Chan, W. W. (1991). Shear wave splitting and subcontinental mantle deformation. *Journal of Geophysical Research*, *96*, 16429–16454. https://doi.org/10.1029/91JB00899

Silver, P. G., & Long, M. D. (2011). The non-commutivity of shear wave splitting operators at low frequencies and implications for anisotropy tomography. *Geophysical Journal International*, *184*(3), 1415–1427. https://doi.org/10.1111/j.1365-246X.2010.04927.x

Silver, P. G., & Savage, M. K. (1994). The interpretation of shear-wave splitting parameters in the presence of two anisotropic layers. *Geophysical Journal International*, *119*(3), 949–963. https://doi.org/10.1111/j.1365-246X.1994.tb04027.x

Skemer, P., & Hansen, L. N. (2016). Inferring upper-mantle flow from seismic anisotropy: An experimental perspective. *Tectonophysics*, *668–669*, 1–14. https://doi.org/10.1016/j.tecto.2015.12.003

Stanley, R. S., & Ratcliffe, N. M. (1985). Tectonic synthesis of the Taconian orogeny in western New England. *Geological Society of America Bulletin*, *96*(10), 1227–1250. https://doi.org/10.1130/0016-7606(1985)96<1227:TSOTTO>2.0.CO;2

van Staal, C. R., Barr, S. M., & Percival, J. A. (2012). Lithospheric architecture and tectonic evolution of the Canadian Appalachians and associated Atlantic margin. *Tectonic styles in Canada: The LITHOPROBE perspective: Geological Association of Canada Special Paper*, *49*, 55.

van Staal, C. R., Whalen, J. B., Valverde-Vaquero, P., Zagorevski, A., & Rogers, N. (2009). Pre-Carboniferous, episodic accretion-related, orogenesis along the Laurentian margin of the northern Appalachians. *Geological Society, London, Special Publications*, *327*(1), 271–316. https://doi.org/10.1144/SP327.13

Wagner, L. S., Fischer, K. M., Hawman, R., Hopper, E., & Howell, D. (2018). The relative roles of inheritance and long-term passive margin lithospheric evolution on the modern structure and tectonic activity in the southeastern United States. *Geosphere*, *14*, 1385–1410. https://doi.org/10.1130/GES01593.1

Wagner, L. S., Long, M. D., Johnston, M. D., & Benoit, M. H. (2012). Lithospheric and asthenospheric contributions to shear-wave splitting observations in the southeastern United States. *Earth and Planetary Science Letters*, *341*, 128–138. https://doi.org/10.1016/j.epsl.2012.06.020

Walsh, E., Arnold, R., & Savage, M. K. (2013). Silver and Chan revisited. *Journal of Geophysical Research: Solid Earth*, *118*, 5500–5515. https://doi.org/10.1002/jgrb.50386

White-Gaynor, A. L., & Nyblade, A. A. (2017). Shear wave splitting across the mid-Atlantic region of North America: A fossil anisotropy interpretation. *Geology*, *45*(6), 555–558. https://doi.org/10.1130/G38794.1

Wintsch, R. P., Sutter, J. F., Kunk, M. J., Aleinikoff, J. N., & Dorais, M. J. (1992). Contrasting P-T-t paths: Thermochronologic evidence for a Late Paleozoic final assembly of the Avalon Composite Terrane in the New England Appalachians. *Tectonics*, *11*, 672–689. https://doi.org/10.1029/91TC02904

Wirth, E., & Long, M. D. (2010). Frequency-dependent shear wave splitting beneath the Japan and Izu-Bonin subduction zones. *Physics of the Earth and Planetary Interiors*, *181*, 141–154. https://doi.org/10.1016/j.pepi.2010.05.006

Withjack, M. O., Schlische, R. W., & Olsen, P. E. (1998). Diachronous rifting, drifting, and inversion on the passive margin of central eastern North America: An analog for other passive margins. *AAPG Bulletin*, *82*(5), 817–835. https://doi.org/10.1306/1D9BC60B-172D-11D7-8645000102C1865D

Withjack, M. O., Schlische, R. W., & Olsen, P. E. (2003). Relative timing of CAMP, rifting, continental breakup, and basin inversion: Tectonic significance. In W. E. Hames, J. G. McHone, P. R. Renne, & C. Ruppel (Eds.), The Central Atlantic Magmatic Province, Insights from fragments of Pangea (Vol. *136*, pp. 33–59). American Geophysical Union, Geophysical Monograph. https://doi.org/10.1029/136GM03

Yang, B. B., Liu, Y., Dahm, H., Liu, K. H., & Gao, S. S. (2017). Seismic azimuthal anisotropy beneath the eastern United States and its geodynamic implications. *Geophysical Research Letters*, *44*, 2670–2678. https://doi.org/10.1002/2016GL071227

Yuan, H., & Levin, V. (2014). Stratified seismic anisotropy and the lithosphere-asthenosphere boundary beneath eastern North America. *Journal of Geophysical Research: Solid Earth*, *119*(4), 3096–3114. https://doi.org/10.1002/2013JB010785

Zen, E. A. (1983). Exotic terranes in the New England Appalachians—limits, candidates, and ages: A speculative essay. In Contributions to the Tectonics and Geophysics of Mountain Chains (Vol. 158, pp. 55–81). GSA Memoir. https://doi.org/10.1130/MEM158-p55